Univerzita Karlova
Přírodovědecká fakulta

Studijní program: Chemie
Studijní obor: Chemie

Pavlína Marková

Hydrofilní blokové kopolymery s navázanou fenylboronovou kyselinou: syntéza, tvorba nanočástic a interakce s funkčními dioly

Phenylboronic acid-containing double hydrophilic block copolymers: synthesis, self-assembly and interaction with functional diols

Bakalářská práce

Školitel: Ing. Mariusz Marcin Uchman Ph.D.
Konzultant: doc. RNDr. Pavel Matějíček, Ph.D.

Praha, 2020

Prohlášení:

Prohlašuji, že jsem závěrečnou práci zpracovala samostatně a že jsem uvedla všechny použité informační zdroje a literaturu. Tato práce ani její podstatná část nebyla předložena k získání jiného nebo stejného akademického titulu.

V Praze, 14. 08. 2020 …….……

I would like to kindly thank all members of the Soft Matter research group for the amicable atmosphere and continuous guidance throughout the first three years of my academic journey at Charles University, especially my supervisor Ing. Mariusz Uchman, Ph.D., and my advisor doc. RNDr. Pavel Matějíček, Ph.D., for their insightful advice and dedicated time. I would like to express my profound gratitude to all the lecturers for passing on their expertise and inspiring me to strive for more profound scientific knowledge. I am also most thankful to my family who has always believed in me and offered me unwavering support throughout my studies.

Abstrakt

Bakalářská práce se zaměřuje na postpolymerizační modifikaci pH responzivních, dvojitě hydrofilních kopolymerů s bloky polyethylenoxidu a poly-4-vinylpyridinu pomocí 2-bromomethyl-4-fluorofenylboronové kyseliny, která je schopna dynamicky vázat funkční dioly a reagovat na vnější podněty. Byla předvedena reprodukovatelná kvaternizační reakce s volitelným stupněm kvaternizace potvrzeným pomocí protonové nukleární magnetické rezonanční spektroskopie a infračervené spektroskopie. Dále bylo sledováno samouspořádávání ve vodných roztocích a tvorba micel, které byly charakterizovány pomocí statického, dynamického a elektroforetického rozptylu světla a mikroskopie atomových sil. Polymerní micely vykazovaly fluorescenci a jejich fotofyzikální vlastnosti byly studovány metodami UV-Vis a fluorescenční spektroskopie.

Abstract

This thesis focuses on the post-polymerization modification of a pH-responsive double hydrophilic diblock copolymer poly(ethylene oxide)-*b*-poly(4-vinyl pyridine) by stimuli-responsive diol-binding 2-bromomethyl-4-fluorophenylboronic acid for potential application in the delivery of functional diols. A reproducible quaternization reaction was performed and the optional degree of quaternization was confirmed by proton nuclear magnetic spectroscopy and infrared spectroscopy. The self-assembly behaviour was investigated and formed micelles were characterized by static, dynamic and electrophoretic light scattering and atomic force microscopy. The polymeric micelles exhibited fluorescence and their photophysical properties were studied by UV-Vis and fluorescence spectroscopy.

Abbreviations

AAS – atomic absorption spectroscopy

AFM – atomic force microscopy

ATRP – atom transfer radical polymerization

CMC – critical micelle concentration

DHBC – double hydrophilic block copolymer

DLS – dynamic light scattering

DMF – N,N-dimethylformamide

ELS – electrophoretic light scattering

EPR – enhanced permeability and retention

FPBA – 2-bromomethyl-4-fluorophenylboronic acid

FTIR – Fourier transform infrared spectroscopy

HIV – human immunodeficiency viruses

HeLa – immortal cell line from cervical tumor of Henrietta Lacks

IR - infrared

LS – light scattering

MWCO – molecular weight cut-off

NMR – nuclear magnetic resonance

P2VP – poly(2-vinyl pyridine)

P4VP – poly(4-vinyl pyridine)

PBA – phenylboronic acid

PBS – phosphate-buffered saline

PEO – poly(ethylene oxide)

PMDETA – N,N,N′,N″,N″-pentamethyldiethylenetriamine

Q25, Q50, Q100 – PEO-*b*-P4VP modified by FPBA with 24, 54 and 92% of quaternization

SEC – size-exclusion chromatography

SLS – static light scattering

THF – tetrahydrofurane

UV – ultraviolet

Table of contents

1. Introduction

Double hydrophilic block copolymers have shown much promise as smart materials for the ever fast-developing field of nanomedicine. Their self-assembly behaviour presents a high-throughput and low-cost method for nanofabrication. However, a thorough understanding of the principles guiding this process and the effect of external stimuli applicable to the studied material is essential for practical applications. The combination of the stimuli-responsive behaviour of double hydrophilic block copolymers with the unique chemical properties of functional groups such as the pH-responsive diol-binding phenylboronic acid entails opportunities for the preparation of nanocarriers for biomedical applications, for instance, targeted drug delivery.

Many nature-derived compounds containing a 1,2- and 1,3-diol functionalities exhibit salubrious properties and are investigated as anticancer therapeutic agents. Nonetheless, in many cases, low-solubility and cytotoxic side effects pose an obstacle to their direct use. To surmount such drawbacks, immobilization in biocompatible polymeric micelles via a pH-responsive dynamic covalent bond with phenylboronic acid can be utilized. Following known criteria for the nanocarriers, the nanomedicine takes advantage of the EPR effect to selectively target tumor tissue. The acidic microenvironment of tumor tissue causes the self-immolation of the pH-responsive links and the functional diol is readily liberated to freely diffuse towards the active site.

In this thesis, a reproducible quaternization reaction is presented for the post-polymerization modification of the commercially available double hydrophilic diblock copolymer poly(ethylene oxide)-*b*-poly(4-vinyl pyridine) by a stimuli-responsive diol-binding 2-bromomethyl-4-fluorophenylboronic acid. The fluorinated derivative displays pK_A closer to the physiological range in comparison to phenylboronic acid and provides ^{1}H, ^{11}B and ^{19}F NMR spectroscopic handles. The degree of quaternization can be selected even though high degrees above 90% are hardly achievable due to unfavourable electrostatic repulsion of neighbouring modified chains. Proton nuclear magnetic spectroscopy and infrared spectroscopy were used to confirm the intended degree of quaternization. Furthermore, the self-assembly behaviour was investigated and formed micelles were characterized by static, dynamic and electrophoretic light scattering and atomic force microscopy. The polymeric micelles exhibited fluorescence and their photophysical properties were studied by UV-Vis and fluorescence spectroscopy.

This thesis is a part of long-term interdisciplinary research of self-assembled block copolymer colloids and encapsulation of low-molar-mass compounds in polymeric nanoparticles in Soft Matter Group. Hereby, I'd like to acknowledge the help and cooperation of research group members and other colleagues: the diblock copolymers were quaternized by Jana Vojtová, Ph.D., NMR spectra were measured with the help of Vladimír Ďorďovič, Ph.D., the method of FTIR spectroscopy was demonstrated by Somdeb Jana, Ph.D., Ph.D. student Anastasiia Murmiliuk assisted with the AFM measurements and AAS was performed by RNDr. Jakub Hraníček, Ph.D.

The financial support of the Czech Science Foundation Grant No. 17-00289Y and the Ministry of Education and Youth and Sport of Czech Republic project LTAIN19078 within the Inter-Excellence program is gratefully acknowledged.

2. Problematics overview

2.1 Double hydrophilic block copolymers

Self-assembly is a process in which a system's nanoscale building blocks organize into ordered structures or patterns without external direction on account of their specific, local interactions.[1,2] Among the synthetic systems which possess the ability to form such ordered nanostructures, amphiphilic block copolymers are of indisputable importance and they have been extensively studied due to the vast range of their possible applications. More recently, a relatively new class of polymeric materials has gained much interest as stimuli-responsive materials. Double hydrophilic diblock copolymers (DHBCs) are composed of two hydrophilic blocks, typically one neutral block such as poly(ethylene oxide) or poly(2-oxazoline)[3] and the other polyelectrolyte, for instance, polyanionic poly(acrylic acid) or poly(vinyl pyridine) as a polycation. Another possibility is a polyzwitterionic polymer with balanced cationic and anionic groups.[4] The block architecture such as the choice of monomers and the length of individual blocks greatly affects the properties of the resulting polymer and careful planning is therefore essential.

2.1.1 Poly(vinyl pyridine) and poly(ethylene oxide)

Two isomers of the neutral poly(vinyl pyridine) block, the poly(2-vinyl pyridine) (P2VP) and poly(4-vinyl pyridine) (P4VP), have been employed in the synthesis of block copolymers. Despite their structural similarity, significant differences originate from the change in the position of the nitrogen heteroatom within the aromatic pendant group.[5] In contrast to P4VP, the lone pair of pyridinyl nitrogen in P2VP is sterically hindered by the polymer backbone and thus not suitable for binding with large organic molecules. Furthermore, P4VP shows better miscibility in polar solvents. In water, the solubility of P4VP is pH-dependent. When the pH is lower than 4.8, the pK_A of P4VP,[6] the nitrogens are protonated and the polycation is soluble. On the contrary, in neutral and basic pH, P4VP becomes largely insoluble.

In addition to its superior solubility in water, the poly(ethylene oxide) (PEO) is relatively inert and carries no charge. It has been classified to be 'Generally Regarded As Safe' by the Food and Drug Administration and has been shown to be removed by renal clearance.[7] Its biocompatibility makes it safe to use as a food aditive,[8] in cosmetic products[9] and the pharmaceutical industry.[10] For the above-mentioned reasons, many potential drug nanocarriers have been prepared using PEO building blocks.

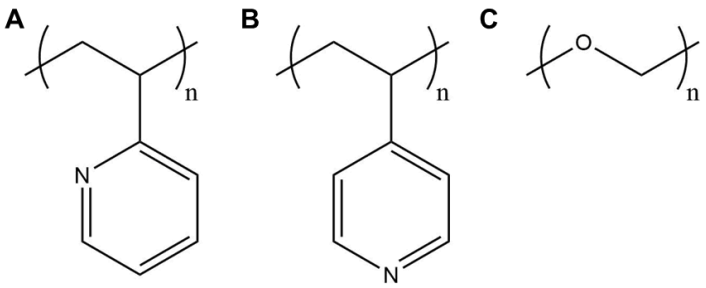

Fig. 1: Structures of (A) P2VP, (B) P4VP and (C) PEO

2.1.2 Self-assembly in aqueous solutions

For the preparation of micellar solutions from a double hydrophilic diblock copolymer PEO-*b*-P4VP, the pH-dependent behaviour of the polyelectrolyte block is exploited. In the bulk state, P4VP is miscible with PEO, whereas phase separation occurs in aqueous media.[5] The P4VP block is rendered hydrophobic by the neutral or basic pH while the PEO block retains solubility throughout the entire pH range. Water serves as a selective solvent because it is a good solvent for the PEO block, however, a precipitant for the P4VP. Consequently, above the critical micelle concentration (CMC), the P4VP forms a compact core which is stabilized by the solvent-swollen PEO corona. Particles can adopt different structures based on the blocks‘ sequences, lengths and volume fractions but also environmental factors such as the pH, temperature and used solvent. The most typical morphologies of diblock copolymers, star-like, crew-cut and cylindrical micelles and vesicles are presented in Fig. 2.

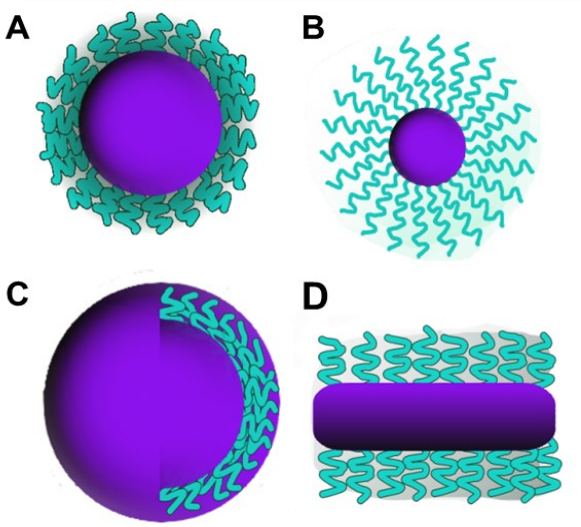

Fig. 2: Illustration of (A) crew-cut, (B) star-like and (D) cylindrical micelle and (C) vesicle morphologies

2.1.3 Application in drug delivery

More than 40% newly developed chemical entities in pharmaceutical industry are practically insoluble in water,[11] hence large part of the DHBC research is focused towards synthesis and characterization of nanocarriers for drug delivery. In comparison to the traditional amphihilic systems, DHBCs’ provide multiple advantages such as enhanced biocompatibility due to fully water-soluble blocks, enhanced permeability of membrane walls even for large cargoes and enhanced degradability or excretion.[12]

On the other hand, one of the main drawbacks of micelle-based nanocarriers is the dependance of their stability on concentration. Upon the injection of nanoparticles into the body, the concentration steeply decreases, diluted by the body fluids. This can cause the concentration to drop bellow the CMC and the dissociation of micelles leads to premature drug release. As a result, concerns for toxicity and delivery efficacy arise. Among the methods to tackle this deficiency, core-crosslinking with degradable crosslinking bonds such as the reversible boronate ester bonds has been investigated.[13,14,15]

2.1.4 Enhanced permeability and retention effect

Nanomedicines and macromolecular drugs have been especially useful for targeted drug delivery to tumor tissues which can reduce the severe side effects of most anticancer agents to normal tissues. An extensive vascular leakage in tumor capillaries makes it possible for nanomedicine to extravasate selectively into tumor tissue.[16] Due to their molecular weight (above 40 kDa), they manage to escape renal clearance and accumulate, while their retention is prolonged by the lack of effective lymphatic drainage. This phenomenon is referred to as the enhanced permeability and retention (EPR) effect.

Heterogeneity of the EPR effect arises from such factors as the patient's pathological, physiological and clinical condition.[17] An increased EPR effect has been reported for hepatocellular and renal cell carcinoma, but most importantly, metastatic tumors which present an ongoing challenge in cancer therapy. To further augment the EPR effect, vascular mediators such as the vasoconstrictor angiotensin II (Fig. 3), have been successfully tested in clinical settings. In contrast to normal tissue, tumor vessels are unable to respond to angiotensin II due to the absence of a smooth muscle layer.[16] Subsequently, the tumor vasculature is mechanically dilated and a 3- to 5-fold increase in blood flow volume is observed.

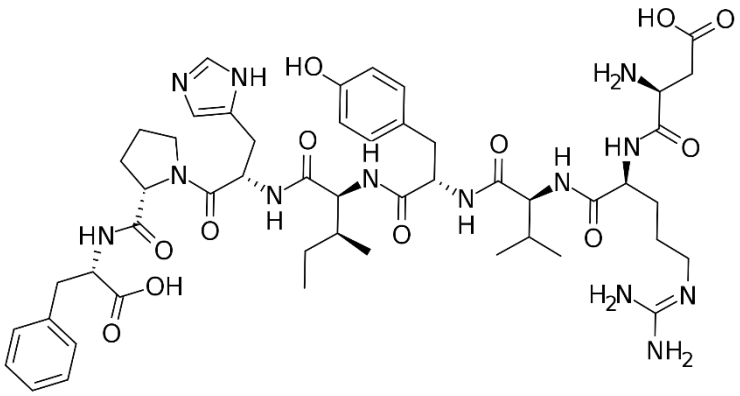

Fig. 3: The structure of vasoconstrictor angiontensin II

The EPR effect is only responsible for targeted delivery to tumor tissues. On the contrary, once the nanomedicine reaches the tumor tissue, the delivery to active sites can be attenuated by its low diffusion constants in comparison to free drugs. The pH (pH 6-6.5) of the tumor microenvironment differs significantly from that of normal tissue and after endocytosis, the intracellular lysosomal pH can be as low as pH 4.[17] Binding the drug via chemical bonds that readily undergo spontaneous hydrolysis under acidic conditions is therefore advantageous in contrast to covalent bonds. For that very purpose, the unique chemical properties of boronic acids can be exploited.

2.2 Phenylboronic acid

Phenylboronic acids (PBAs) are organic compounds derived from the structure of boric acid by substituting one of the hydroxyl groups by phenyl. They are inherently electron-deficient with a vacant p-orbital on the sp^2 hybridized boron atom which gives them properties of a mild Lewis acid. Reactivity and properties can be tuned by altering the substituent.

In aqueous solutions, a pH-dependent equilibrium exists between the neutral hydrophobic form in which the three substituents adopt trigonal planar geometry and an sp^3 hybridized hydrophilic hydroxyboronate anion with tetrahedral geometry. The latter is favoured at a pH above the pK_A of the phenylboronic acid (pK_A = 8.9).[18] By a change in pH, the reaction can be reversed in a neutral or acidic environment.

One of the most intriguing properties of PBAs is their ability to form boronate esters by reversibly binding vicinal diols. The formation of esters with 1,2- or 1,3-diols includes many biologically relevant species such as terpenes, prostaglandins or steroids, hence, the PBA has been used as a protecting group for such natural products.[18] Even though the binding occurs for both PBA forms, the esters formed by hydroxyboronate anion exhibit better hydrolytic stability.

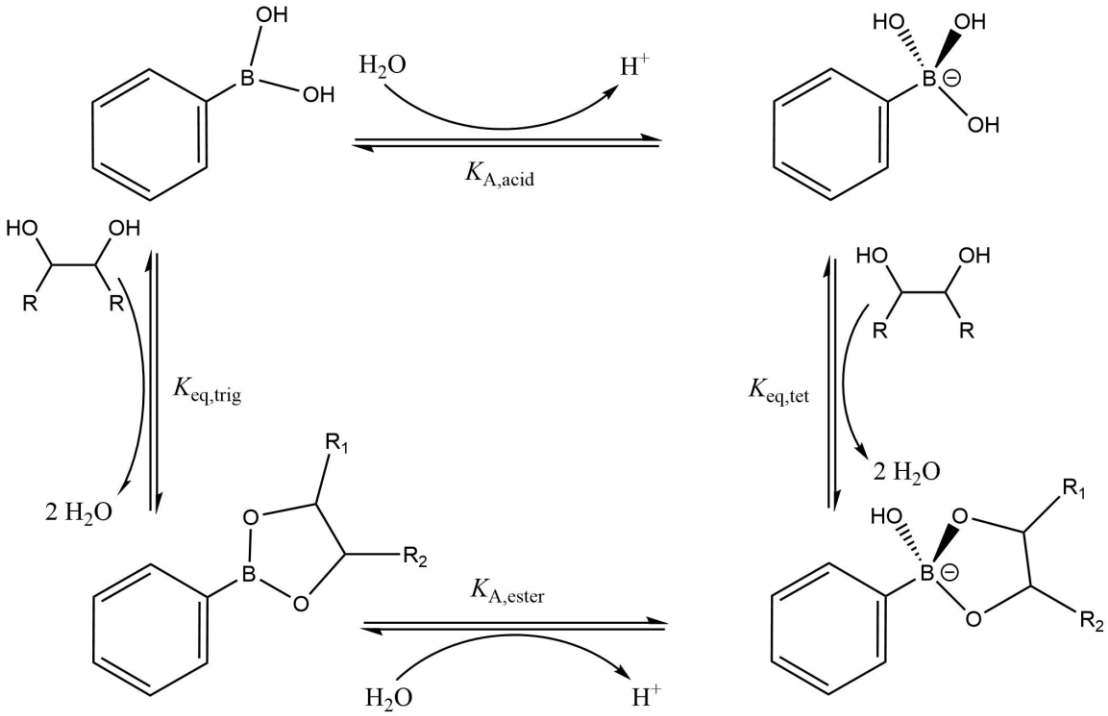

Fig. 4: Trigonal and tetragonal form of PBA reversibly binding vicinal diols

To utilize this behaviour in targeted drug delivery, it is necessary to achieve such effective binding in physiological conditions. That requires shifting the pK_A of PBA closer towards the range of physiological pH. Functionalization of the phenyl ring with an electron-withdrawing group such as fluorine has proven to lower the pK_A to 8.77,

8.09 and 7.89 for 4-fluorophenylboronic acid, 3-fluorophenylboronic acid and 2-fluorophenylboronic acid respectively.[19]

The pK_A of the formed boronate ester is considerably lower in comparison to the free PBA. For instance, when mannitol is added into an aqueous solution of PBA, its pK_A is gradually decreasing until a minimum corresponding to the pK_A of the mannitol ester is reached (pK_A = 5.78).[20]

Due to their unique chemical properties, an abundance of polymeric materials for biomedical applications has been functionalized with boronic acids. Recently, binary codes enabling DNA-like sequence recognition of macromolecules have been based on the dynamic covalent interaction between PBAs and catechols.[21] More traditional examples of the purpose of incorporated boronic acid group are as follows; it can respond to the overexpression of reactive oxygen species as a cleavable hydrophobic group rendering the free polymer hydrophilic, its glucose-sensing behaviour can be utilized for dynamic insulin release or as a targeting moiety for specific saccharides on cell membranes and the pH-responsive behaviour can be used to trigger the disassembly of the nanocarriers or as a self-immolative linker for the therapeutic agent.[22]

2.3 Crocin and gossypol

It has been recognized that fruits, vegetables, herbs and spices are natural sources for numerous anticarcinogenic agents.[23] Among them, compounds endowed with 1,2- and 1,3-diols can be used as crosslinking agents between phenylboronic acid-containing polymer chains. The pH-responsive nature of the formed ester bonds allows these therapeutic agents to be readily liberated in the acidic microenvironment of the tumor tissue.

Crocin is a plant-produced tetraterpenoid-based organic pigment that makes up about 25% of saffron and is responsible for its colour.[24] The disugar ester has shown many salubrious properties as an antioxidant, radical scavenger and inhibitor of the growth of cancer cells.[23] A large number of cancer types have been shown to be affected by saffron extract such as skin, cervical, breast and lung carcinoma.[25] An apoptosis mechanism of the cytotoxic effect on HeLa cells was discovered.[23]

Gossypol is a yellow polyphenolic pigment isolated from cottonseed. It has shown interesting biological activity, for example as an inhibitor of HIV replication and male antifertility agent.[26] Its role as a promising potential anticancer drug for several breast tumor cell lines has been reported.[27] However, the low solubility of this hydrophobic compound and considerable toxicity pose an obstacle for its direct use in therapy. Strategies employed to overcome these drawbacks include immobilization in micelles or a controlled release from PBA-modified hydrogel matrix.[28]

2.4 Characterization techniques

2.4.1. Light scattering

Static light scattering

Light scattering occurs when the oscillating electric field of the impinging light causes a shift in the electric-charge distribution of the particles.[29,30] The charges within these particles move at the same frequency as the external electric field, thus they are turned into oscillating dipoles whose emitted radiation is seen as scattered light. Isotropic scatterers, molecules sufficiently smaller compared to the wavelength of the incident light, undergo so-called Rayleigh scattering. In this case, the intensity of the scattered light is almost invariant with respect to direction and the wavelengths of the incoming and scattered light are the same.

However, once larger particles are concerned, phase variations take place leading to the development of interference effects. As a result, by studying how the intensity of the scattered light changes as a function of the scattering angle θ, it is possible to extract information on the size and shape of the particles in question. On this principle, the static light scattering (SLS) technique is based. To ensure simplicity of some of the equations, it is more convenient to substitute the scattering angle θ with the scattering vector $\vec{q}$. As a photon is being scattered after a collision with a particle, its wavevector $\overrightarrow{k_{\text{in}}}$, a vector pointing in the direction of the propagation, changes, $\overrightarrow{k_{\text{out}}}$. The scattering vector is then defined as:

$$\vec{q} = \overrightarrow{k_{\text{out}}} - \overrightarrow{k_{\text{in}}} \tag{1}$$

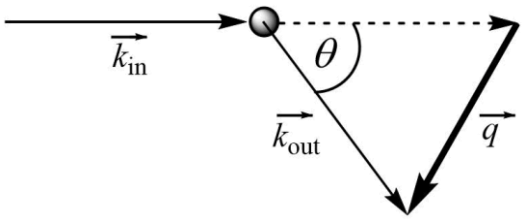

Fig. 5: Definition of the scattering vector

Figure 5 illustrates that the length of the scattering vector can be expressed as:

$$q = 2 \cdot k \cdot \sin\frac{\theta}{2} \tag{2}$$

Using the length of the wavevector $k = 2\pi / \lambda$ and the relationship between the wavelength of light in the medium and the one in vacuum $\lambda = \lambda_0 / n$, formula (2) can be rewritten in the most conventional form:

$$q = \frac{4\pi n}{\lambda_0} \cdot \sin\frac{\theta}{2} \tag{3}$$

To eliminate the influence of the apparatus factors on the measured scattered intensity, a normalized quantity called Rayleigh ratio is introduced:

$$R(q) = \frac{I_s(q)r^2}{I_0 V_s(q)} \quad (4)$$

Where $I_s(q)$ is the intensity of the scattered light measured, I_0, is the intensity of the laser, $V_s(q)$ is the scattering volume and r is the distance from the scattering volume to the detector.

The information about molecular weight, shape of the particles and their interaction can then be derived from the general equation for SLS:

$$\frac{Kc}{R(q)} = \frac{1}{MP(q)}(1 + 2A_2 MP(q)c + \dots) \quad (5)$$

where K is a constant proportional to the square refractive index increment $\mathrm{d}n/\mathrm{d}c$, c is the weight concentration of molecules, M is the molecular weight, $P(q)$ is the form factor and A_2 is the second virial coefficient.

The second virial coefficient A_2 reflects the nature of interactions between particles in a solution. If no interparticle forces are present, the value of the coefficient would be equal to zero, repulsive forces are then represented by a positive value while attractive by a negative one. The form factor $P(q)$ is a correction factor which could be interpreted as the ratio between the scattering intensity of the studied particles and the scattering intensity of some hypothetical particles of the same molecular weight but infinitely small dimensions. With a suitable approximation, the radius of gyration R_g, an average distance of mass elements of the molecule from its center of mass, can be determined.

To work out the molecular weight, it is necessary to measure $R(q)$ for multiple samples that are gradually more and more diluted, at several decreasing values of q. Through a series of extrapolations to zero values for concentrations and eventually the scattering vector, it is possible to obtain the sought-after quantity. To perform this data fitting graphically, the so-called Zimm plot is utilized and will be discussed in more detail in the experimental section 4.2.4.

Dynamic light scattering

While in SLS, the average intensity of the scattered light as a function of the scattering vector is measured, another technique called dynamic light scattering (DLS) takes advantage of the temporal fluctuations in the intensity to ascertain the diffusion coefficients of the particles in which size information is embedded indirectly.[29,30] The constructive and destructive interference arising from the phase difference between emitted waves results in maxima and minima in the scattered intensity focused in specific directions. Nevertheless, the thermal density fluctuations of the solvent molecules induce random, uncontrolled movement of the studied particles which is referred to as the Brownian motion, and that causes the intensity measured by the detector to fluctuate.

Using a digital autocorrelator, a vast amount of calculations is being carried out simultaneously to calculate the normalized intensity autocorrelation function g_2 from which

the diffusion coefficient D can be derived. The diffusion coefficient is indicative of the particle's mobility which is directly related to its physical dimensions. The larger the particle is, the larger the friction it needs to surmount. For spherical particles, this is demonstrated by the Stokes' equation:

$$F_{\mathrm{fr}} = 6\pi\eta r \tag{6}$$

Customarily, the experimentally determined diffusion coefficient is inserted into the Stokes-Einstein (7) relation to calculate the hydrodynamic radius. It is the radius of a hypothetical spherical particle with the same diffusion coefficient, including the solvation layer.

$$R_{\mathrm{h}} = \frac{kT}{6\pi\eta D} \tag{7}$$

The two introduced LS techniques are complementary and often used conjointly.

2.4.2. Infrared spectroscopy

Along with the Raman spectroscopy, infrared spectroscopy plays a pivotal role in probing the vibrational states of molecules.[31,34] Even at the temperature of absolute zero, atoms in a molecule vibrate about their equilibrium positions. The potential energy of a diatomic molecule as a function of internuclear separation in the vicinity of equilibrium extension of the bond R_{e} can be expressed using a Taylor series:

$$V(x) = V(0) + \left(\frac{\mathrm{d}V}{\mathrm{d}x}\right)_0 x + \frac{1}{2}\left(\frac{\mathrm{d}^2V}{\mathrm{d}x^2}\right)_0 x^2 + \frac{1}{6}\left(\frac{\mathrm{d}^3V}{\mathrm{d}x^3}\right)_0 x^3 + \cdots \tag{8}$$

The equilibrium corresponds to the minimum of potential energy, therefore, the first derivative is equal to zero. Setting the term $V(0)$ arbitrarily to zero and neglecting higher-order terms, the dependence of potential energy V on momentary distance R in a diatomic molecule can be approximated by a parabola for small displacements x from equilibrium:

$$V(x) = V_0 + \frac{1}{2}k(R - R_{\mathrm{e}})^2 = V_0 + \frac{1}{2}kx^2 \tag{9}$$

where k is the force constant related to the curvature of the potential energy close to the equilibrium which can be also interpreted as the stiffness of the bond.

The relative motion of two atoms with the masses m_1 and m_2 and parabolic potential energy can be described by the same Schrödinger equation as the linear harmonic oscillator:

$$-\frac{\hbar^2}{2m_{\mathrm{eff}}}\frac{\mathrm{d}^2\Psi}{\mathrm{d}x^2} + \frac{1}{2}kx^2\Psi = E\Psi \tag{10}$$

where $m_{\mathrm{eff}} = m_1m_2 / (m_1 + m_2)$ is the effective mass and Ψ is the wavefunction of the studied system. By solving this equation, we obtain the vibrational wavefunctions as well as the discrete vibrational energy levels.

A transition between an initial vibrational state $\Psi_{\upsilon_{\mathrm{i}}}$ and a final vibrational state $\Psi_{\upsilon_{\mathrm{f}}}$ is only electric-dipole allowed with a non-zero transition dipole moment:

$$\mu_{\mathrm{fi}} = \int \Psi_{\upsilon_{\mathrm{f}}}{}^{*}\,\hat{\mu}\Psi_{\upsilon_{\mathrm{i}}}\,d\tau \equiv \left\langle \Psi_{\upsilon_{\mathrm{f}}} \middle| \hat{\mu} \middle| \Psi_{\upsilon_{\mathrm{i}}} \right\rangle \tag{11}$$

Should the dependence of μ on x be expressed using a Taylor series, the gross selection rule for a change in vibrational state as well as the specific selection rule can be derived; the dipole moment of the molecule must change in the course of the vibration for it to be IR active and $\Delta\upsilon = \pm 1$.

The transition wavenumber can be calculated using the following expression:

$$G(\upsilon + 1) - G(\upsilon) = \frac{E(\upsilon+1) - E(\upsilon)}{hc} = \left(\upsilon + \frac{3}{2}\right)\tilde{\nu} - \left(\upsilon + \frac{1}{2}\right)\tilde{\nu} = \tilde{\nu} \qquad (12)$$

Parabolic approximation performs poorly when higher excitation energies are concerned and it does not take into consideration possible dissociation of the bond. For a more precise description of vibrational terms, the anharmonic oscillator model can be utilized. Some of the possible approaches include retaining the higher-order terms in the potential energy Taylor series or using a function more accurately reproducing the shape of the potential energy curve, such as the Morse potential. The energy levels are no longer equidistant but converge with the increasing vibrational quantum number, there is a finite number of vibrational levels and transitions with $\Delta\upsilon = \pm 2, \pm 3, \ldots$ are also allowed which accounts for the presence of overtones in the absorption spectra. Vibrational transitions are also accompanied by the rotational ones, which results in the splitting of each absorption line to a number of adjacent components.

The infrared spectra of polyatomic molecules are much more complex due to the presence of multiple vibrational modes. For a nonlinear N-atomic molecule, there are $3N-6$ independent vibrational modes. Such modes, in which all atoms vibrate with the same frequency and in phase and no translation or rotation of the molecule as a whole is involved, are called normal modes. In a good approximation, each one can be treated as an independent harmonic oscillator oscillating with its own frequency. Any vibrational state of the molecule is specified by $3N-6$ vibrational quantum numbers. Typically, the most intensive bands in the IR spectra are the fundamental bands that represent the fundamental transition, $1 \leftarrow 0$. Weaker absorption bands corresponding to transitions $2 \leftarrow 0$, $3 \leftarrow 0$,… are denoted as overtones. If more than one vibrational quantum number changes simultaneously, such bands are termed combination bands.

Absorption bands of certain atomic groups can be found in a relatively narrow interval of wavenumbers, such as hydroxyl or carbonyl functional groups. They vibrate almost independently of the rest of the molecules and these characteristic vibrations can be used to interpret the IR spectra and identify the molecules. Most spectral databases use complicated patterns in the fingerprint region at lower wavenumbers to identify the molecule.

In Fourier transform infrared spectroscopy, a polychromatic beam of light is passed through Michelson interferometer prior to interacting with the sample. The spectral information is acquisited in the form of an interferogram in which the measured intensity is a function of the optical path difference. A spectrum in the frequency domain is obtained by mathematical operation, the Fourier transform. This method is advantageous due to the mechanical simplicity of the spectrometer, improved speed of measurement and a reduction of signal-to-noise ratio in the output spectra.

IR spectroscopy has an immense number of applications in both research and industry. In polymer science, examples of these include a physical method

of microstructural investigations regarding double bonds determination in the isomer analysis of polybutadiene, experimental determination of sequence distribution in copolymers or tacticity determination.[32]

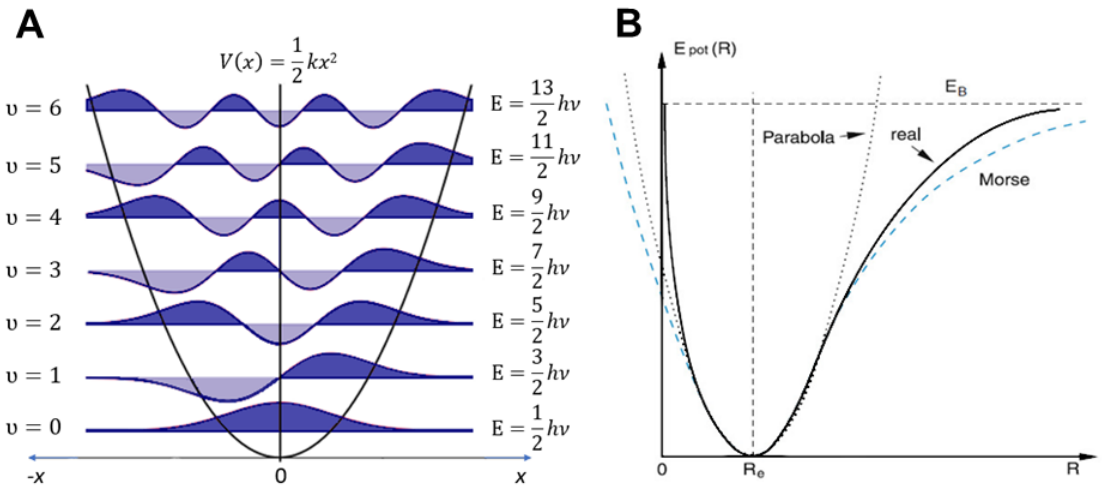

Fig. 6: Visual representation of (A) wavefunctions obtained from solving Schrödinger's equation in the harmonic oscillator model and (B) parabolic and Morse potential curves and their deviation from the real (experimentally obtained) potential curve[33]

2.4.3. Nuclear magnetic resonance spectroscopy

A nucleus is NMR active provided it has a non-zero spin quantum number, I.[31,34] The magnitude of an angular momentum of such a nuclei is then defined as:

$$|I| = \hbar\sqrt{I(I+1)} \tag{13}$$

with a corresponding magnetic moment:

$$\mu_I = \frac{g_N \mu_N}{\hbar} I = \gamma I \tag{14}$$

where g_N is the nuclear g-factor, $\mu_N = e\hbar / 2m_p$ is the nuclear magneton, $\hbar$ is the reduced Planck constant and the constant of proportionality γ is the gyromagnetic ratio, an empirically determined characteristic of the nucleus dependent on its internal structure.

In classical physics, the energy of a magnetic moment μ in a magnetic field with the magnetic induction B is given by the scalar product of these two vectors. In like manner, in quantum mechanics it is expressed by the interaction Hamiltonian:

$$\hat{H} = -\hat{\mu} \cdot B = -\gamma \hat{I} \cdot B \tag{15}$$

The z-component of angular momentum is equal to the eigenvalues of the operator $\hat{I}_z = m_I\hbar$, where $m_I = (-I, -I+1, \ldots, I-1, I)$ is the magnetic quantum number.

Since the static external magnetic field B_0 of an NMR spectrometer is conventionally directed along the z-axis of the laboratory coordinate system, the corresponding energies can be obtained using the following equation:

$$E_{m_I} = -\gamma \hat{I}_z \cdot B_0 = -\gamma \hbar m_I B_0 \tag{16}$$

This separation of the degenerated spin levels in magnetic field is called the nuclear Zeeman effect. If the oscillating electromagnetic field is perpendicular to the static magnetic field and the selection rule $\Delta m_I = \pm 1$ is followed, the transition can be stimulated by absorption of electromagnetic radiation. For resonance to occur, the energy of the photons in the electromagnetic field must match the transition energy. Among the most commonly studied nuclei, ^{1}H, ^{13}C, ^{19}F and ^{31}P all have a spin quantum number $I = 1/2$. As shown in Fig. 7, the energy of a photon required to excite such transition is:

$$\Delta E = \frac{1}{2}\gamma \hbar B_0 - (-\frac{1}{2}\gamma \hbar B_0) = \gamma \hbar B_0 \tag{17}$$

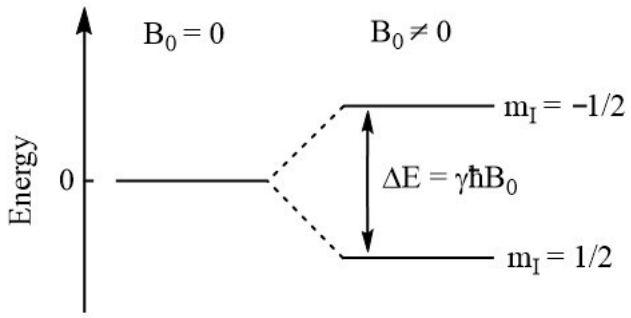

Fig. 7: Separation of the degenerated spin levels in magnetic field

According to Planck's law, the frequency satisfying this resonance condition, also called Larmor frequency, must be equal to:

$$\nu_0 = \frac{\Delta E}{h} = \frac{\gamma B_0}{2\pi} \tag{18}$$

However, because the local magnetic field is a superposition of the external magnetic field and the opposing internal magnetic field induced by the surrounding cloud of circulating electrons, not all nuclei of a certain isotope resonate at the exact same frequency. The effective field at the *i*-th nucleus can be expressed as:

$$B_{i,\text{eff}} = (1 - \sigma_i) B_0 \tag{19}$$

where σ_i is the shielding constant of the *i*-th nucleus. Since the shielding is quite small compared to the magnitude of the static magnetic field and it is dependent on the experimental setting, it is more convenient to define a new quantity known as the chemical shift δ:

$$\delta = \frac{\nu - \nu_{\text{ref}}}{\nu_{\text{ref}}} \tag{20}$$

which references the resonance frequency of the sample ν against the resonance frequency of a standard compound ν_{ref} measured in the same applied magnetic field and is usually given in ppm.

Heteronuclear J-coupling is an indirect spin-spin interaction mediated by the valence electrons of the two NMR active nuclei. Such an effect takes place between the ^{1}H and ^{11}B nuclei and it is responsible for the splitting of the ^{1}H signal into a 1:1:1:1 quartet. By irradiating these nuclei, fast transitions between the spin levels are induced and their effective spin is zeroed out. The so-called ^{11}B decoupling can be performed to simplify the ^{1}H NMR spectra as illustrated by Fig. 8.

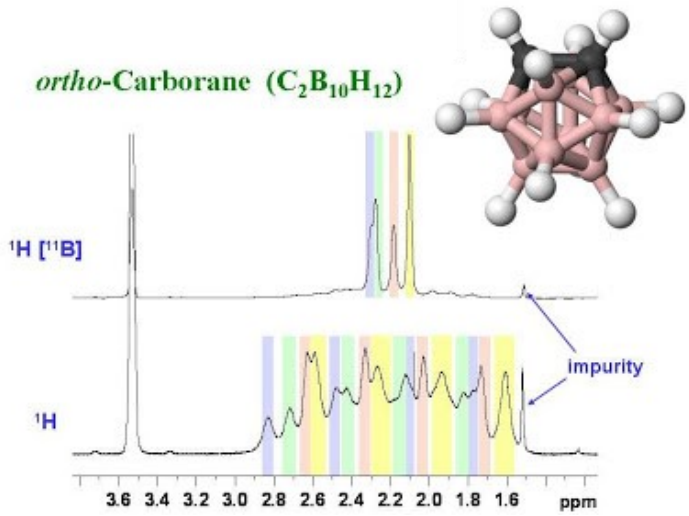

Fig. 8: ^{1}H NMR spectra of ortho-carborane acquired with and without ^{11}B decoupling[35]

In comparison to low molecular organic compounds, a broad absorption line is generated by a superposition of numerous individual resonances. The considerable number of protons in a slightly different magnetic environment make interpretation of polymer ^{1}H NMR spectra quite challenging. Nonetheless, NMR spectroscopy still plays a substantial role in the characterization of polymers. It can be used as an absolute method of mass determination by end-group analysis.[36] Other possible application include experimental determination of tacticity and long-chain or short-chain branching.[32] The fraction of the immobilized polymeric segments can also be studied. While the highly mobile chain segments form narrow lines in the ^{1}H NMR spectra, the peaks of the immobilized segments appear to be significantly broadened or disappear completely.[37]

3. Aims of thesis

This thesis is a part of long-term interdisciplinary research of self-assembled block copolymer colloids and encapsulation of low-molar-mass compounds in polymeric nanoparticles in Soft Matter Group, the Department of Physical and Macromolecular Chemistry, Charles University. The aims of this thesis are as follows:

1. To prepare a stimuli-responsive phenylboronic acid-containing double hydrophilic diblock copolymer via post-polymerization quaternization reaction of the poly(ethylene oxide)-*b*-poly(4-vinyl pyridine), PEO-*b*-P4VP, with 2-bromomethyl-4-fluorophenylboronic acid.
2. To characterize and quantify the post-polymerization quaternization reaction efficiency utilizing NMR and IR spectroscopy.
3. To investigate the self-assembly behaviour of the modified diblock copolymers in aqueous solutions and characterize the formed micelles in terms of size and molecular mass.
4. To probe the photophysical changes in the solution of polymeric micelles prior to and after the addition of drug-crosslinking agents crocin and gossypol.

The obtained knowledge will allow for reproducible preparation of double hydrophilic diblock copolymer with incorporated stimuli-responsive diol-binding boronic acid functionalities and further studies of their potential application as nanocarriers in transport of functional diols, for instance, targeted drug delivery.

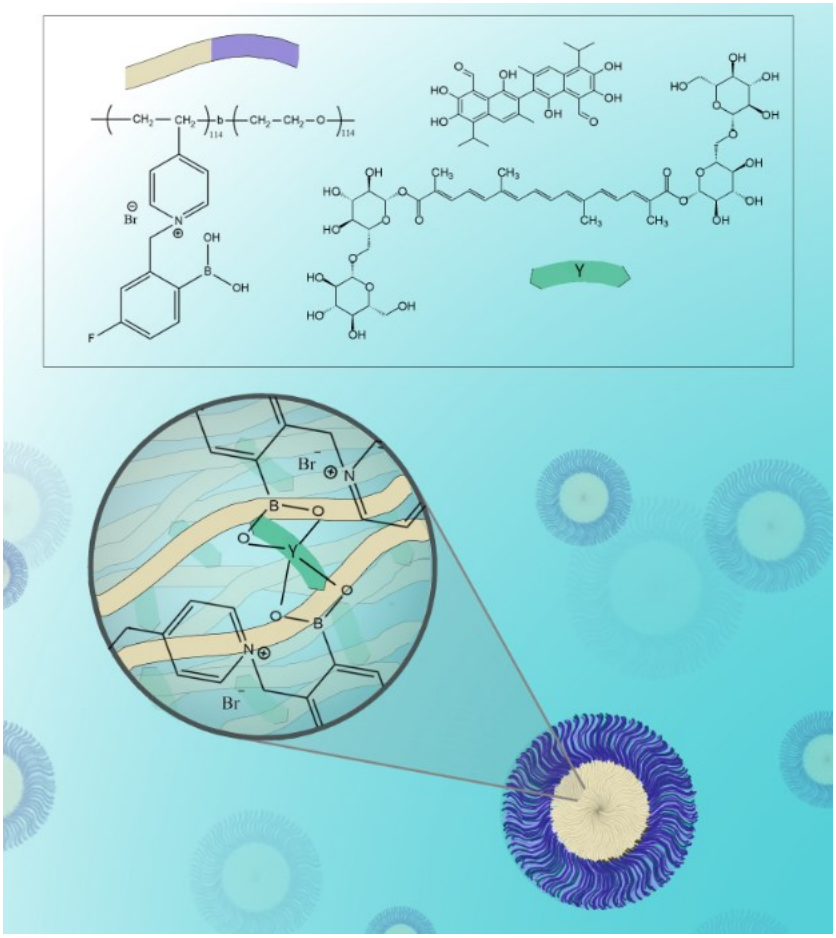

Fig. 9: Illustration of the drug-crosslinked polymeric micelle

4. Materials and methods

4.1 Used materials and chemical substances

The block copolymer poly(ethylene oxide-*b*-4-vinyl pyridine), PEO-*b*-P4VP, was purchased from Polymer Source Inc. (Canada). It was prepared via atom transfer radical polymerization (ATRP) with bromo-terminated poly(ethylene glycol) methyl ether as a macroinitiator and methoxy group terminating the PEO polymer chain. Fig. 10 shows a schematic representation of the synthesis procedure.

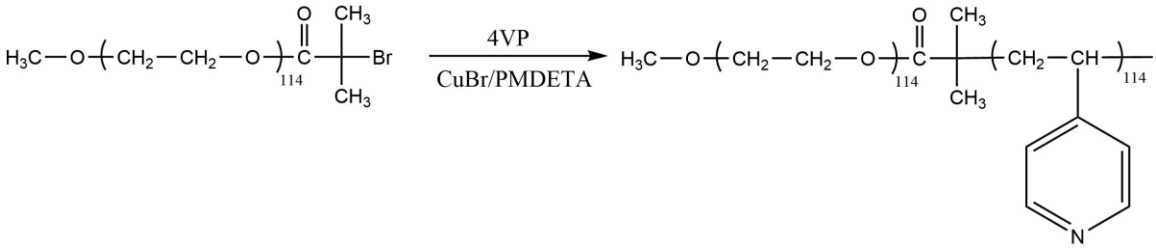

Fig. 10: Schematic representation of the synthesis of PEO-b-P4VP

The number average molecular weight Mn of 5000-*b*-12000 and the molecular weight distribution Mw/Mn represented by dispersity *Đ* of 1.20 was determined by size exclusion chromatography (SEC) in dimethylformamide (DMF) as a mobile phase. The PEO/P4VP ratio 1/1 was confirmed by ^{1}H NMR spectra as discussed in section 5.2.1.

The 2-bromomethyl-4-fluorophenylboronic acid, FPBA, with the molecular weight of 232.8 g/mol and 95% purity was purchased from Combi-Blocks, Inc. (United States). Its structure is shown in Fig. 11.

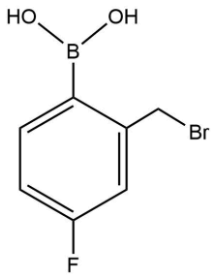

Fig. 11: Structure of 2-bromomethyl-4-fluorophenylboronic acid

The samples for NMR spectroscopy measurements were prepared using deuterated solvents: D_2O (99.9 atom % D, SigmaAldrich, United States), DCl (20% in D_2O, 99.5 atom % D, Chemotrade, Germany), NaOD (30% in D_2O, 99.3 atom % D, Chemotrade, Germany) and MeOD (99.8 atom % D, SigmaAldrich, United States).

Spectrum™ Spectra/Por™ 1 RC Dialysis Membrane Tubing (Spectrum Chemical Mfg. Corp., United States) with the nominal molecular weight cut-off (MWCO)

of 6000-8000 Da, flat width 32 mm and diameter 20.4 mm was used for dialysis. CupriSorb was purchased from Seachem Laboratories, Inc. (United States).

Water was purified by Barnstead™ MicroPure™ water purification system (Thermo Scientific™, United States). It was used to prepare solutions: 0.1M HCl by diluting 35% hydrochloric acid (Lach-Ner, s.r.o., Czech Republic) and 0.1M NaOH by dissolving NaOH beads (PENTA s.r.o., Czech Republic).

The phosphate-buffered saline (PBS) buffer was prepared by dissolving PBS tablets (SigmaAldrich, United States). One tablet per 200 mL of deionized water yielded 0.01M phosphate buffer, 0.0027M potassium chloride and 0.137M sodium chloride, pH 7.4 at 25 °C.

The pH meter was calibrated using Orion™ pH buffers (pH 4.01 and 10.01, Thermo Scientific™, United States). Crocin (purity for microscopy, 976.96 g/mol) was purchased from SigmaAldrich (United States) and gossypol-acetic acid (98%, 578.61 g/mol) from AvaChem Scientific (United States). All compounds were used as received.

4.2 Used methods and sample preparation

4.2.1 Modification of PEO-*b*-P4VP by FPBA

To study the influence of PEO-*b*-P4VP modification by FPBA on the polymer behaviour and properties, polymer samples of three different degrees of quaternization, 25%, 50% and 100%, further denoted as Q25, Q50 and Q100 respectively, were prepared. The weighed amounts of reactants are recorded in Table 1.

Table 1: Quaternization of PEO-P4VP, where m_{pol} is the weight of the nonmodified polymer with the corresponding amount of substance n_{pol}, the amount of substance of P4VP groups to be quaternized n_{P4VP}, the calculated weight of pure FPBA m_{pFPBA} and the corresponding weight m_{FPBA} of the 95% FPBA available.

	m_{pol} (mg)	n_{pol} (μmol)	n_{P4VP} (mmol)	m_{pPBAF} (mg)	m_{PBAF} (mg)
Q100	200	11.765	1.3411	312	328
Q50	300	17.647	1.0059	234	246
Q25	320	18.824	0.5365	125	131

All of the quaternization processes were carried out in an identical manner,[38] thus only the synthesis of Q100 will be presented herein. The schematic representation of the polymer modification is shown in Fig. 12.

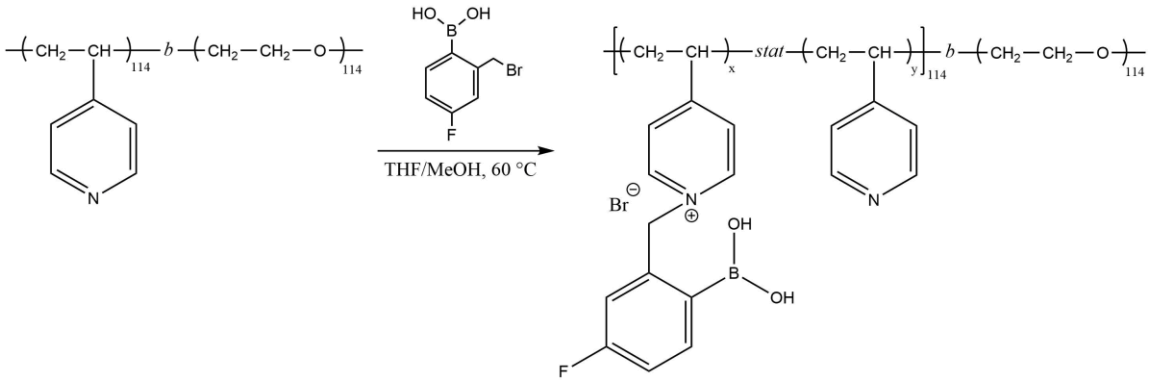

Fig. 12: Schematic representation of the PEO-b-P4VP modification by FPBA

200 mg of PEO-*b*-P4VP was weighed into a 50 mL round bottom flask and dissolved in 5 mL of dried tetrahydrofuran. A molar equivalent of FPBA, 312 mg, was dissolved in 1 mL of dry tetrahydrofuran and added to the PEO-*b*-P4VP solution. The flask with the reaction mixture was then sealed with a polytetrafluoroethylene septum, purged with argon and heated to 60 °C. The mixture was homogenized by the addition of 3 mL of methanol and stirred by a magnetic stir bar for 3 days.

For the product to precipitate, the yellow reaction mixture was added dropwise to 15 mL of cold diethyl ether in a 50 mL beaker. The suspension was filtered through a glass frit and the precipitate was washed with 10 mL of diethyl ether three times. Subsequently, it was dissolved in a solution of 6 mL of methanol with 1 mL of water. CupriSorb was added and the mixture was left stirring overnight. The suspension was again filtered and the precipitate was dried using a vacuum desiccator. The product was isolated in the form of 440 mg of a light yellow solid which represented a yield of 86%.

In the reaction with Q25, no methanol was added because the product seemed to be dissolved forming a yellow solution. For each sample, the yield, appearance and quaternization calculated from ^{1}H NMR as discussed in section 5.2.1 is recorded in Table 2 and Fig. 13 provides photo-documentation.

Table 2: Description of products of quaternization reactions. PEO-b-P4VP modified by FPBA. The degree of quaternization was determined by ^{1}H NMR spectroscopy.

	Yield (mg)	Yield (%)	Appearance	Quaternization (%)
Q100	440	86	Light brown solid	92
Q50	465	87	Brown solid	54
Q25	399	90	Light yellow solid	24

10 mg of each sample was weighed into a vial and 5 mL of 0.1M HCl and subsequently in a new vial with the same amount of sample 5 mL of 0.1 M NaOH was added to investigate their solubility under acidic and basic conditions.

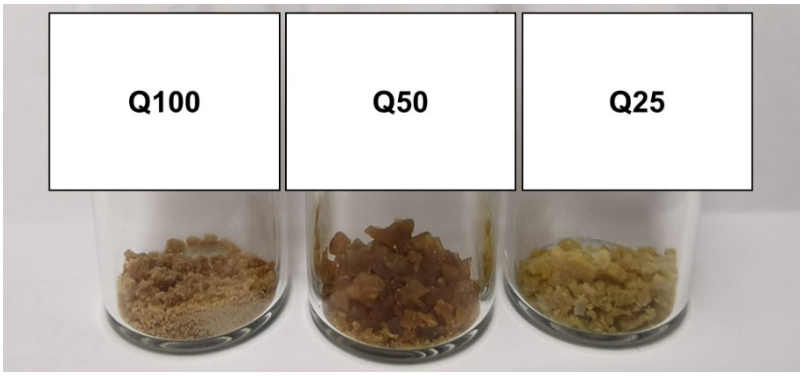

Fig. 13: Solid products Q100, Q50 and Q25 of quaternization reactions of PEO-b-P4VP with FPBA with the intended degree of quaternization 100, 50 and 25% respectively

4.2.2 NMR spectroscopy

^{1}H and ^{11}B NMR measurements were performed Varian Unity Inova 400 MHz spectrometer and ^{19}F NMR measurements using Bruker 400 MHz spectrometer. A saturated solution of boric acid in D_2O with the chemical shift 19.5 ppm was used to reference the ^{11}B signals,[39] other NMR spectra were referenced to the signals of their solvents. To avoid the signal arising from the borosilicate glass of the NMR tube, quartz tubes were used for the measurements, however, a boron-containing NMR probe is responsible for a broad signal found in the ^{11}B NMR spectra.

^{1}H NMR spectra for determination of the degree of quaternization were measured in MeOD/D_2O mixture. The quaternized polymer only dissolved upon the addition of a few drops of 30% DCl.

An 0.1M solution of DCl was prepared by diluting 20% DCl with D_2O. 0.7 mL of this solution was added to 0.7 mg of nonmodified polymer, Q25, Q50 and Q100. The Q25 and polymer samples dissolved quickly. Most of Q50 dissolved during the next few hours and the resulting solution was apparently scattering light. The Q100 in the white, milky solution did not even dissolve overnight. A small amount of MeOD was added to aid the dissolution and ^{1}H NMR spectra were recorded.

An 0.1M solution of NaOD was prepared by diluting 30% NaOD with D_2O. 7 mg of Q100 were dissolved in 0.7 mL and the colour of the solution changed to reddish brown. In the same manner, a sample of Q25 was prepared. ^{1}H and ^{11}B NMR spectra were collected repeatedly. Within 24 hours, the Q25 precipitated. The NMR tube was left standing at the desk. In two weeks, three separate regions were observed within the tube. The top was richly yellow, middle part which was shaded by a rubber band with from a tag to label the sample was green and the bottom part was light yellow. Upon tilting the tube, the darker part started coming down creating a helix-like shape. Needle was used to pull out the sample in a gel-like form which was both elastic and sticky.

4.2.3 Fourier transform infrared spectroscopy

Prior to the sample preparation, all the necessary equipment was cleaned with acetone and dried. Approximately 4 spatulas of potassium bromide were homogenized in a mortar. The fine-grained white powder was then grinded with a portion of sample with the sample to bromide ratio of about 1:100 and thoroughly mixed. Manual powder tablet press machine Trystom H62 was used to mold half of the powder into a tablet. 70 kN were applied for 2 to 3 minutes. The finished tablet was then carefully removed. Should it not fit the required standards, the other half of the powder was used to recreate it without the need to repeatedly prepare the sample mixture.

The Fourier transform infrared spectroscopy measurement was performed using the Thermo Nicolet Magna 760 IR instrument equipped with a Chem Inspector IR microscope module and the OMNIC software. The cover of the instrument was removed and the background was collected in the default transmission mode. Subsequently, the tablet was secured in a holder that was placed into the instrument so that the laser would intersect with it in the middle. The IR spectra of the sample were collected and automatic baseline correction was applied. The data for each sample were saved in both transmission and absorption mode to be analyzed and plotted in Origin.

4.2.4 Static and dynamic light scattering

The light scattering measurements (SLS and DLS) were performed on a photometer (ALV, Germany) consisting of CGS-3 automatic goniometer, a 7004 multitau multibit autocorrelator, two high-QE APD pseudo cross-correlation detectors, and a 100 mW, 660 nm diode-pumped solid-state laser (Cobolt AB, Sweden). It was operated via ALV-Correlator Software V.3.0. 1 mL of the prepared solution was transferred into cleaned and with a compressed air duster dusted tubes via 0.45 μm membrane filter using a 1 mL syringe. To prevent undesirable losses, the filter was always washed with a few drops of solvent first. For Zimm plot measurements, 1 mL of a concentrated solution of the sample was filtered and 400, 300, 200 and 100 μL were transferred into tubes which were then topped up to 1 mL with the respective pre-filtered solvent to avoid multiple filtrations.

The measurements were taken at 26 °C with the duration of 10 s and the range of scattering angles from 30° to 150° by the angular step of 10°. Considering the probability distribution each angle was measured three times and only the averaged intensity values were used for further calculations. The instrument was pre-calibrated using a file for the toluene standard with a well-known Rayleigh ratio and since aqueous solutions of low concentrations are of interest, pre-recorded water file was used instead of a particular solvent for all measurements. Individual samples were prepared at least a day before the actual measurements took place and were left overnight in the proximity of the instrument to reach equilibrium and not to be excessively disturbed by further transfer.

Next, for four different concentrations of each sample measured at multiple angles, double extrapolation to zero concentration and zero angle was performed using the Alvstat software. By neglecting the higher-order terms in the equation (5), a simplified Zimm equation can be derived:

$$\frac{Kc}{R} = \frac{1}{MP(q)} + 2A_2c \tag{21}$$

The form factor $P(q)$ can be approximated by 1 for sufficiently small scattering vectors which is why the extrapolation to zero scattering angle was carried out. The slope of Kc/R ($\theta = 0°$, c) is then equivalent to the second virial coefficient increased by a factor of 2. When a second approximation to a zero concentration is conducted, the obtained y-intercept represents a reciprocal value of the true molecular weight.

The slope Kc/R of over q^2 is used to determine the form factor $P(q)$ which contains information about the radius of gyration. The Zimm equation relates them as reads:

$$\frac{1}{P(q)} = 1 + \frac{q^2 R_g^2}{3} \tag{22}$$

By fitting the data from dynamic light scattering, the diffusion coefficient of studied particles was obtained. Stokes-Einstein equation (7) allowed for recalculation to the hydrodynamic radius, R_h, which is usually used for its easier visualisation. The ratio between the two radii, R_g to R_h, which is referred to as the shape factor was calculated to rougly approximate the shape of the micelles.

4.2.5 Dialysis against water and PBS

The dialysis membrane tubing was cut to approximately 15 cm long pieces. These were placed into a large 1L beaker filled with regular sink water and heated to 60 °C while stirring on a magnetic stirrer for 30 minutes. The softened tubing was thoroughly rinsed with deionized water and stored in a dilute sodium azide solution. Prior to use, the membrane was repeatedly rinsed with deionized water to remove all the traces of the sodium azide solution and cut to form a single layer sheet to cover the microdialysis capsule.

10 mg of Q100, Q50, Q25 and nonmodified polymer was weighed into a vial and dissolved in 5 mL of 0.1M hydrochloric acid. The transparent solution was then transferred into capsules. Once the prepared membranes were fixed in place by capsule closure, they were submerged into 800 mL of a PBS buffer or 800 mL of deionized water respectively. The buffer solution was prepared by dissolving 4 tablets in 800 mL of deionized water. The capsule was set in rotation by a magnetic stirrer and the dialysis fluid was exchanged 3 times, first after an hour and a half, second after 3 hours and the third was left overnight.

The next day, the samples were carefully removed from the capsule through the pierced membrane using a 1 mL syringe. For samples that were dialysed against water, slight changes in the volume were observed. The pH of the aqueous solution as well as the original solution in 0.1M hydrochloric acid was measured using an Orion Star A211 pH meter (Thermo Scientific™, United States) and recorded into Table 3. These samples were subsequently used for zeta potential measurements that will be discussed in the next section.

Table 3: pH of samples in 0.1 M HCl and water. The first were directly dissolved in acid. The aqueous solution was prepared by dissolution of polymer in 0.1M HCl and dialysis against water.

	pH (HCl)	pH (H_2O)
polymer	1.03	4.56
Q25	0.95	4.95
Q50	0.95	5.66
Q100	0.91	5.24

The Q50 precipitated forming a gel-like precipitate the colour of grey tinged with green when dialysed against phosphate-buffered saline. The Q100 in PBS was intensively scattering light and both Q25 and nonmodified polymer in PBS also showed signs of scattering visible by the naked eye although with a lower intensity. Due to the occurrence of intense scattering, the solutions for light scattering measurements were diluted 100 times and filtered via 0.45 μm membrane filter. However, the dilution proved to be too excessive as the instruments did not show presence of any scatterers.

Next, the solutions were only diluted 5 times to the concentration of 0.4 mg/mL. The nonmodified polymer and Q25 samples were still visibly scattering light but it was still possible to measure them. Surprisingly, there was no apparent scattering of the Q100 sample and the instrument only recorded a very low intensity of scattering while the attenuator was 100% open. A new sample of Q100 diluted 3 times to the concentration of 0.7 mg/mL was finally suitable for LS measurements.

4.2.6 Zeta potential measurements

The zeta potential measurements were based on electrophoretic light scattering (ELS) and performed using a Nano-ZS Zetasizer (Malvern Instruments, UK). 1 mL of the studied sample was transferred into a disposable plastic cuvette by an automatic pipette. The cuvette was placed into the instrument and capped with the reusable zeta dip cell which was thoroughly rinsed with water and dried in between samples. The solution was tempered to 20 °C and the results were collected as an average of 5 consecutive measurements each consisting of 10 runs with 5 seconds of delay in between.

The applied electric field caused the charged particles to migrate towards an electrode of opposite polarity. This electrokinetic process is referred to as electrophoresis. The shift in frequency of the light scattered from particles in motion is used to determine the electrophoretic mobility. Zeta potential, a potential at the hydrodynamic plane of shear known as the slipping plane of an electric double layer, is then obtained from these electrophoretic mobilities using the Henry equation in the Smoluchowski approximation:

$$\mu = \frac{\varepsilon\zeta}{\eta} \tag{23}$$

where μ is the electrophoretic mobility, ε is the dielectric constant of the solvent and η is the viscosity of the solvent.

A titration experiment was performed using 2 mL of Q25 in 0.1M HCl. First, the solution was filtered using an 0.45 μm membrane filter. The pH was gradually adjusted by small additions (a few μL) of filtered 1M NaOH.

4.2.7 Atomic force microscopy

Atomic force microscopy measurements were performed in the tapping mode under ambient conditions using an NT-MDT Ntegra Prima scanning probe microscope, equipped with a Nanosensors silicon cantilever. Samples were prepared by fast dip coating of a freshly peeled out mica surface in dilute micellar solution in 0.1M HCl (circa 0.5 mg/mL). After the evaporation of water, the samples were dried in a vacuum oven at ambient temperature for approximately 1 hour.

The AFM measurements were operated and the obtained scans further analyzed using NovaTM software NT-MDT Solver NOVA 1.1.0.1851. The average was fitted within the one-dimensional Flatten Correction and the 3rd order surface was subtracted within the two-dimensional Flatten Correction prior to data evaluation.

4.2.8 UV-Vis spectroscopy

The absorbance measurements were performed on Shimadzu UV-Vis spectrophotometer in 1 cm pathway quartz cuvettes at a slow speed rate in the wavelength range from 280 nm to 700 nm at room temperature. Water was used as a blank for all dilute aqueous solutions.

4.2.9 Fluorescence spectroscopy

The measurements were performed using Fluorolog FL 3-22 fluorometer (Horiba Jobin Yvon, France) equipped with double grating excitation and emission monochromators, a FluoroHub time-correlated single photon counting module and a TBX single photon counting detector. Steady-state fluorescence measurements used a 450 W high-pressure xenon arc lampas a light source.

During the emission measurements, the samples in 1 cm pathway quartz cuvettes were excited at 350 nm, with the excitation slit open to 3 nm and the emission slit to 2 nm, the emission spectra were collected in the wavelength range from 360 to 600 nm. For excitation measurements, the excitation range was from 250 to 430 nm by the increment of 1 nm, with the excitation slit open to 2 nm and the emission slit to 3 nm. The integration time was set to 0.5 nm/s.

5. Results and discussion

5.1 Solubilization of the modified polymers

The solubility of the quaternized polymer was investigated. In 0.1M hydrochloric acid, all the samples were soluble in a matter of minutes and the resulting solution was transparent and colourless.

The longterm stability of these solutions is attributed to the positive charge on P4VP groups. In the acidic environment, protonation takes place and aids the solubility of the otherwise less hydrophilic P4VP blocks. The Q100 was the last to dissolve which correlates to the number of nonmodified P4VP available for protonation. Even though quaternization places a permanent positive charge on the P4VP nitrogen, the hydrophobic effect of fluorine-modified PBA prevails.

Conversely, once 0.1M sodium hydroxide was used as a solvent, the Q100 started to dissolve first producing a green solution. The dissolution of Q50 resulted in a slightly ligher green solution which was the least stable and started precipitating in a span of an hour. The Q25 took the most time to dissolve, the yellowish green colour was only hinted in the solution which was stable at first, but precipitation occurred the next day.

Within the span of a week, both the precipitated polymers formed a membrane-like structure which was removed in one piece using tweezers, gently dried with filtration paper and used as a sample for FTIR spectroscopy.

The reverse trend in comparison to the acidic environment can again be explained by the degree of quaternization. The pH of the basic solution is above the pK_A of PBA which adopts tetragonal form placing a negative charge on boron. Such behaviour both improves solubility and results in prolonged stability of Q100. All the observed changes are recorded in Table 4 and demonstrated in Fig. 14.

Table 4: Solubilization properties of the Q25, Q50 and Q100 in 0.1M NaOH

	Dissolution	Colour of solution	Stability of solution
Q25	very slow	yellowish green	a few hours
Q50	slow	green	an hour
Q100	relatively fast	darker green	longterm

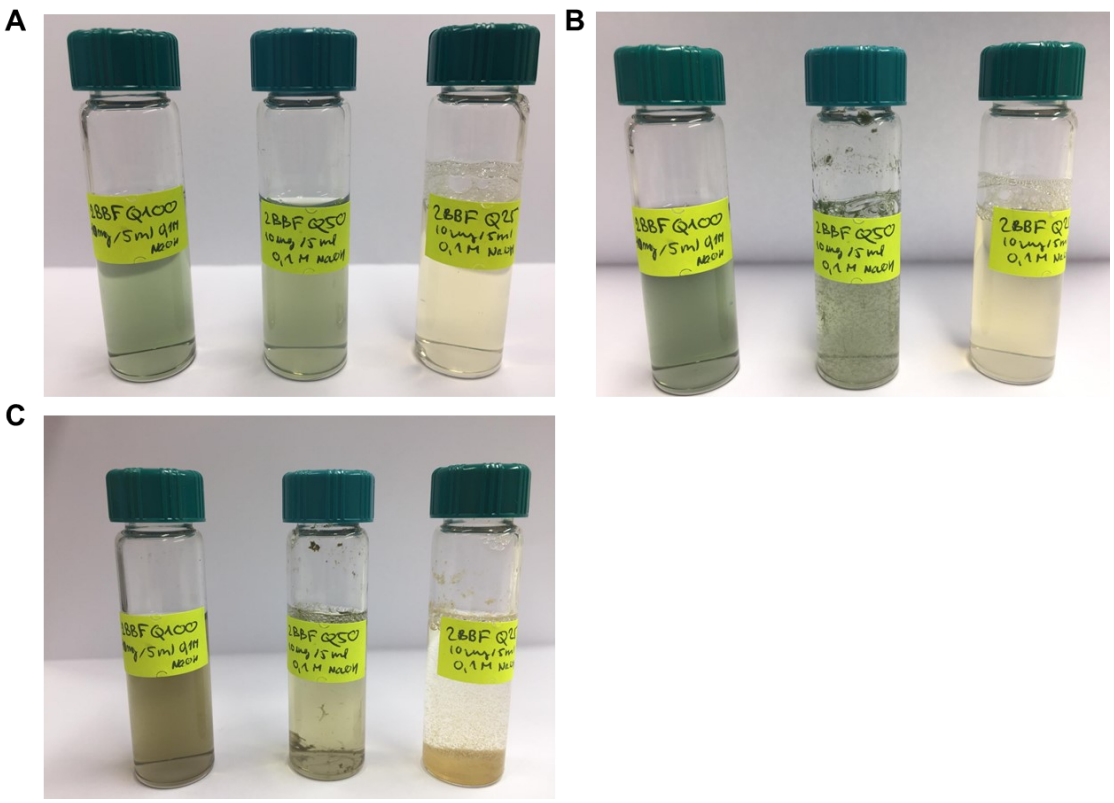

Fig. 14: Precipitation of Q50 and Q25 in 0.1M NaOH. Photos were taken (A) upon dissolution, (B) in an hour and (C) in 14 hours

The different shades of the colouring of the solution seemed to correspond to the degree of quaternization of the respective sample. The green colour could be explained by the presence of traces of copper, a remnant of the catalyst used during the polymer synthesis. In the basic environment of sodium hydroxide, these impurities form the water-insoluble copper(II) hydroxide, which can only be stabilized by the polymer for a limited amount of time and eventually leads to precipitation. However, no copper was detected by elemental analysis.

A more sensitive method with a more favourable detection limit was chosen to verify the stated assumptions. 100 mg of the nonmodified polymer was dissolved in 10 mL of 0.1M hydrochloric acid and measured using the atomic absorption spectroscopy (AAS) by RNDr. Jakub Hraníček, Ph.D., from the Department of Analytical Chemistry, Faculty of Sciences, Charles University in Prague. It was determined that the concentration of copper in the sample was 1.66 µg/ml which is equivalent to 166 µg of copper per g of sample.

To evaluate the possible gravity of impact of such a concentration of copper in the solution, the ratio of poly(4-vinyl pyridine) units to copper atoms present was calculated. The fact that the coordination number of copper can range from 1-6 was also taken into account. Nonetheless, the binding energy is inversely proportional to the coordination number and therefore the lower coordination numbers are viewed as more probable.[40] The results are presented in Table 5.

Table 5: Calculation of the orientational P4VP/Cu ratio per 1 g of sample with n_{pol} and n_{P4VP} being the amount of substance of the polymer and P4VP units respectively. N_{P4VP} and N_{Cu} represent the number of P4VP units and copper atoms. The ratio is calculated for a range of coordination numbers 1-6. The nominal quaternization is considered.

	Q25	Q50	Q100
n_{pol} (μmol)	42.37	33.00	22.99
n_{P4VP} (mmol)	4.830	3.762	2.621
N_{P4VP} (10^{21})	2.909	2.265	1.578
N(Cu) (10^{18})	1.573	1.573	1.573
P4VP/Cu for coordination number:			
1	1849	1440	1003
2	925	720	502
3	616	480	343
4	462	360	251
5	370	288	201
6	308	240	167

The remainder of the solution from AAS analysis and a freshly prepared solution of 100 mg of nonmodified polymer in 10 mL of 0.1M hydrochloric acid were placed in a Spectra/Por tubing and dialysed against pure deionized water with the addition of CupriSorb, a powerful adsorbent of copper. The dialysate was regularly exchanged for two weeks and the resulting sample solution was lyophilized, yielding 148 mg of a very light, white solid. 20 mg of this purified sample was again dissolved in 2 mL of 0.1M hydrochloric acid and the solution was used for AAS analysis. The amount of copper was under the detection limit of this method, meaning the concentration of its traces must have been lower than 0.1 μg/mL.

To perform further trace analysis and determine the exact amount of copper still present in solution, an especially sensitive technique such as anodic stripping voltammetry with the detection limit of $3 \cdot 10^{-9}$ mol/L (0.2 μg/L) would have to be utilized.[41] Even so, that is not within the scope of this thesis and the result from AAS analysis already proved the polymer contained copper impurities that were readily removed by dialysis in the presence of a copper chelating resin.

5.2 Determination of the degree of quaternization

5.2.1 Determination by NMR spectroscopy

^{1}H NMR of nonmodified polymer was measured. In aromatic area, two well-separated peaks (**b**) of the P4VP hydrogens can be observed at 8.38 and 7.42 ppm. This shift to the higher frequencies for an aromatic system is caused by the diamagnetic anisotropy.[34] The circulating π-electrons in a conjugated π-electron system are responsible for a ring current which in turn induces additional magnetic field. The direction of magnetic field induction outside of the ring is in accordance with that of the applied magnetic field. Therefore, protons located outside of the aromatic ring experience a greater effective

magnetic field, which results in a greater separation of their spin levels. To overcome greater energy difference, a photon of higher frequency is required. The electronegativity of nitrogen causes the even more pronounced downfield shift of the peak corresponding to the hydrogens closer to the heteroatom. The P4VP/PEO ratio 1/1 was confirmed by integration of these aromatic hydrogen signals and comparing the sum of their integrals with the integral of PEO signal (**e**) at its characteristic chemical shift 3.6 ppm.[42]

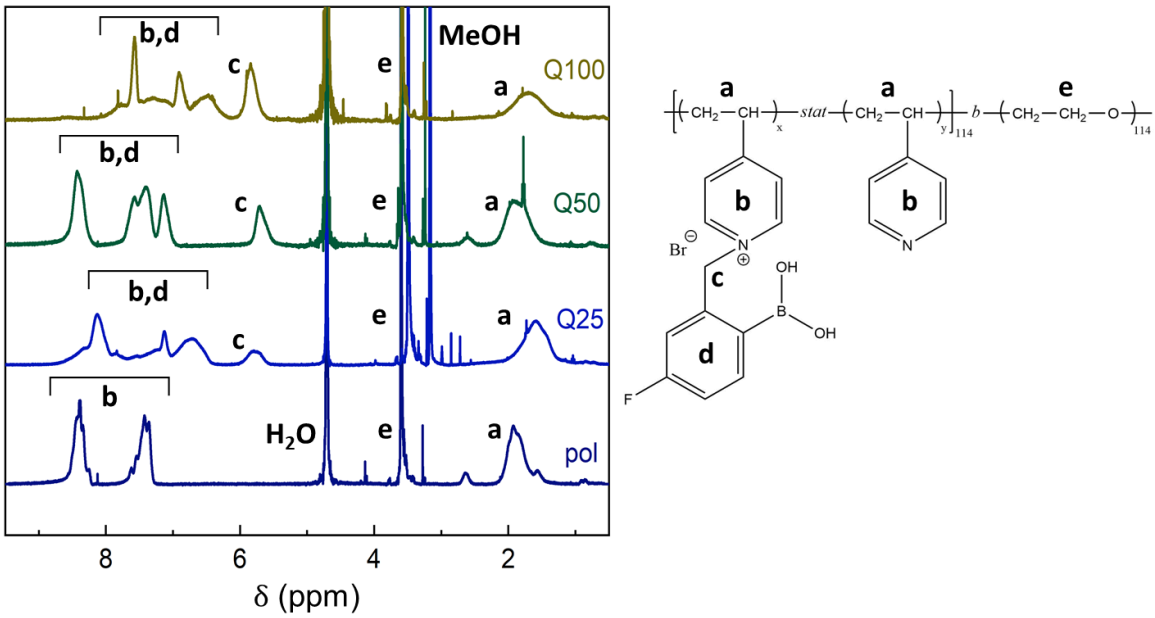

Fig. 15: ^{1}H NMR spectra of PEO-b-P4VP and Q25, Q50 and Q100. Polymer was measured in D_2O, the quaternized samples in MeOD/D_2O with an addition of 30% DCl.

In contrast to the nonmodified polymer, in ^{1}H NMR of Q100 in the acidic solution only the PEO signal was detectable. For Q50 the intensity of the P4VP and FPBA signals was significantly decreased and only Q25 showed well-defined signals for all its segments. This suggests the formation of kinetically frozen nanoparticles with PEO shell stabilized P4VP core in which the core-forming P4VP chains have restricted mobility. When a solution of NaOD was used as a solvent for Q100, the colour of the solution changed to brown with a tinge of red with no apparent scattering which might have been caused by the presence of copper(I) ions. Within an hour, the solution turned to green which could indicate the presence of copper(II) ions and after several days it changed to brown again. The green basic solution was measured and contrary to the acidic conditions, all peaks were detectable in the ^{1}H NMR spectra.

This can be related to the presence of the more hydrophilic anionic phenylboronate species found in basic conditions bellow the pK_A of FPBA and their different solubility as discussed in section 5.1. The transition to the anionic tetrahedral substituted hybridization state is linked to an upfield shift of the ^{11}B and ^{19}F signals (Fig. 16). Due to boron bonding with an additional electron-donating OH group, the distribution of electron density in its proximity changes and even affects the fluorine located on the same phenyl ring. In ^{11}B NMR spectra, the intensity of signal is substantially obscured by the background of the boron-containing NMR probe, however, the shift from approximately 20 ppm to 2 ppm can be observed for both Q100 and Q25. The choice of solvent also affects the intensity greatly as in NaOD the P4VP chains quaternized by FPBA are considerably more mobile. ^{19}F NMR spectra also exhibit sizeable background, regardless, the shift from approximately -107 ppm to -119 ppm is apparent.

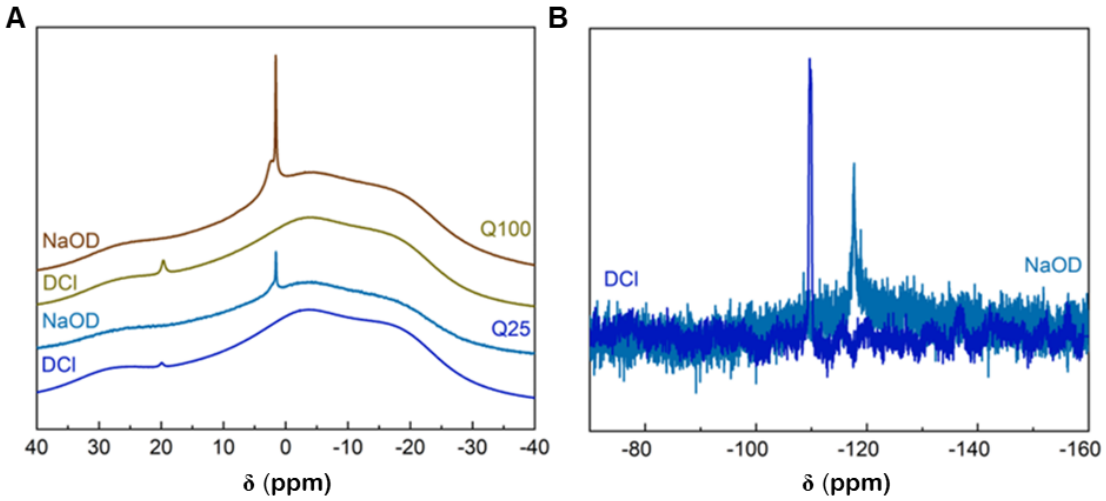

Fig. 16: The chemical shift caused by change from trihedral to tetragonal form of FPBA in (A) ^{11}B NMR spectra of Q100 and Q25 and (B) ^{19}F NMR spectra of Q25. 0.1M DCl and 0.1M NaOD were used as solvents.

For quaternized samples, new peaks appear in the ^{1}H NMR spectra (Fig. 15). The FPBA signal falls into the aromatic region, however, due to the broad character of these peaks, overlapping occurs and the separation becomes quite challenging. The degree of quaternization was therefore calculated using the signal from methylene linker (**c**) connecting FPBA to P4VP block which is present in all the modified polymers. Its integral was compared to the reference integral of a well-defined PEO peak which was chosen due to its superior solubility in all the used solvents. The degrees of quaternization determined by ^{1}H NMR are as follows: 92% for Q100, 54% for Q50 and 24% for Q25.

The Q100 deviates the most from the intended degree of modification. That is consistent with the notion that quaternization becomes gradually more difficult when a high percentage of P4VP units are already modified and more importantly charged. The repulsive interaction between the same charges partially prevents the neighbouring P4VP units from further modification.

5.2.2 Determination by FTIR spectroscopy

The band shift of the pyridine vibrational modes in the infrared absorption spectra can also be utilized to investigate the degree of quaternization of poly(vinylpyridine). Alongside three samples of different degrees of quaternization, Q25, Q50 and Q100, monomeric analogue and nonmodified polymer infrared spectra are compared herein.

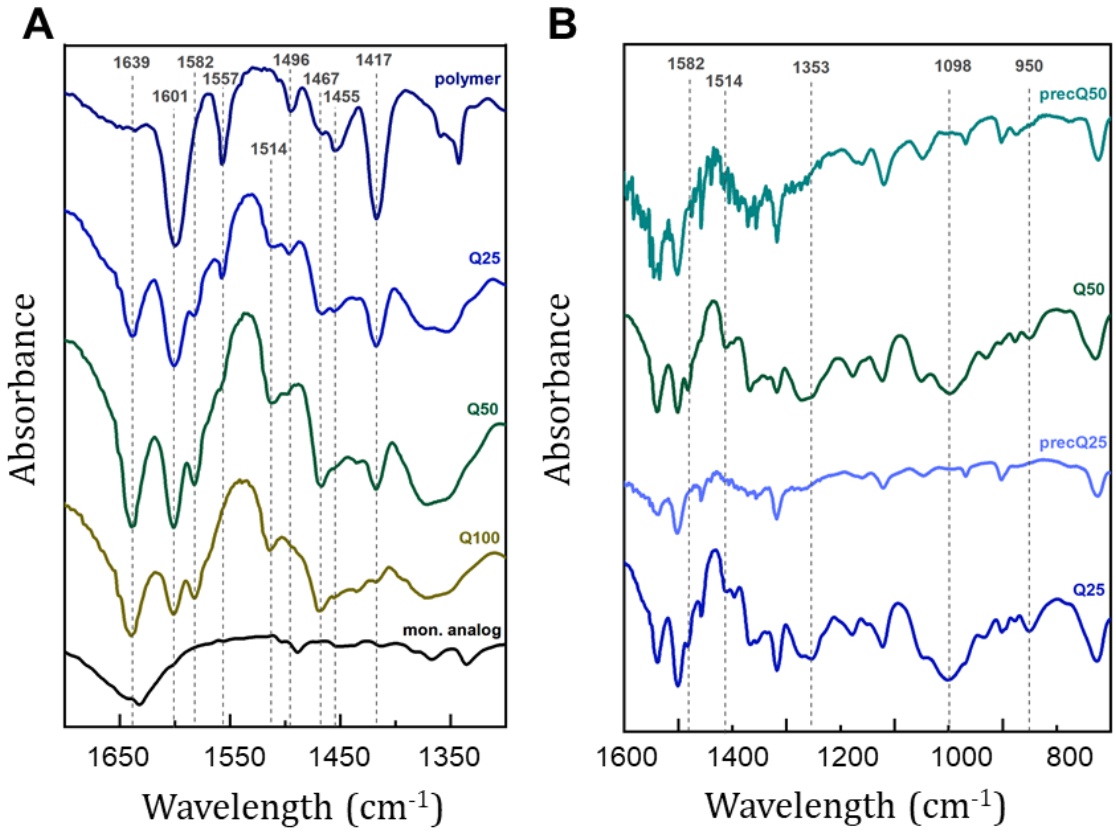

Fig. 17: FTIR spectra (A) of the monomeric analogue, Q25, Q50, Q100 and polymer and (B) of Q25, Q50 and their respective precipitates. The spectra were collected from tablets prepared with KBr. The precipitates formed in 0.1M NaOH.

In the region of higher wavenumbers, 3500-2800 cm^{-1}, bands assigned to the stretching of O-H bond (strong and distinctively broadened, a possible indication of hydrogen bonding between OH groups of nearby PBAs) in phenylboronic acid and aromatic C-H stretching[43] were detected as shown in Table 6. Arguably, N-H stretching might be responsible for the other two peaks in this region. In IR spectra of the polymer, the peak located at 2893 cm^{-1} is very strong but gradually decreases with the increasing degree of quaternization. An opposite trend can be seen for the peak located at higher wavenumbers.

In the wavenumber range of 1650-1400 cm^{-1}, bands corresponding to pyridine groups are centered at 1601, 1557, 1496 and 1417 cm^{-1}.[38,44] When a quaternized pyridinium ring is present, a new peak appears in the IR spectra near 1639 cm^{-1} accompanied by the increasing intensity of the 1467 cm^{-1} peak[44] and changes in the intensity of the above-mentioned bands can be observed.[45,46] Even though the ratio between the intensities of the quaternized pyridinium ring and the uncharged pyridinium group is not directly proportional to their quantities, the change in intensities provides conformation of the increasing degree of quaternization and is in a good agreement with the results from NMR spectroscopy.

Ranging from 1400-1300 cm^{-1}, stretching modes of the B-O bond in phenylboronic acid can be identified.[47] Mode assignment was performed according to the literature[38,43,44,45,46,47,48] but apart from a few distinctive peaks serves more for orientational purposes. More measurements with a variety of differently substituted samples would be needed to support these estimations.

The right-hand side of Fig. 17 shows normalized IR spectra comparing the Q50 and Q25 vibrations with the precipitates from 0.1M NaOH. Several changes can be observed, the most striking is the disappearance of the peaks at 950, 1098 and 1582 cm^{-1}. The intensities of the peaks centered at 1514, 1372 and 1353 cm^{-1} decreased. These suggest structural changes in the proximity of the FPBA functional group. Other methods, such as solid state NMR, could provide additional information.

Table 6: List of the observed vibrational modes for nonmodified polymer sample, modified samples Q25, Q50 and Q100 and quaternized monomer analogue.

pol	Q25	Q50	Q100	mon. an.	Mode assignment
3408	3417	3408	3417	3442	O-H stretching
3068	3126	3123	3123	-	C-H stretching
3049	3039	3043	3043	3057	C-H stretching
3025	2920	2925	2920	-	N-H stretching
2893	2873	2876	2873	-	N-H stretching
-	1638	1640	1639	1631	C=N stretching
1600	1601	1600	1601	-	C=C stretching
-	1583	1582	1582	-	C-C stretching
1557	1557	-	-	-	N-H bending
	1512	1512	1514	-	C-C stretching
1488	1496	1497		1495	C-C stretching
1467	1467	1465	1469	-	C-C stretching

pol	Q25	Q50	Q100	mon. an.	Mode assignment
1360	1374	1371	1372	1366	B-O stretching
1343	1351	1353	1353	1334	B-O stretching
1280	1280	1278	1276	-	C-H bending
1105	1101	1098	1098	-	B-C stretching
826	826	829	831	-	B-O stretching
568	564	557	542	-	in plane BO_2 deformation

5.3 Nanoparticle size and molecular weight determination by LS measurements

Conducting the Zimm analysis is the most convential approach to analysing data collected via light scattering measurements as it can provide useful information about the size and shape of the studied particles. To utilize Zimm equation (21), the refractive index increment d*n*/d*c* must be known in order to calculate the constant *K*. However, the determination of specific refractive index increment represents a complex problem that is influenced by numerous factors such as the wavelength of the used laser, the temperature, studied particle-solvent pair, the particle's conformation or presence of additives in the solvent.[49] Furthermore, it requires a substantial amount of sample.

For all the above-mentioned reasons, measurements are commonly performed with an estimated value of the specific refractive index increment. Such an estimation can affect the obtained values of molecular weight and second virial coefficient and therefore must be employed reasonably. For that purpose, it is possible to make us of the many values for polymers, especially comercially available ones, in various solutions that are tabelized and available in literature.[50]

For newly synthesized or modified block copolymers, the value of refractive index increment can be estimated using the values for individual blocks. In the case of the modified PEO-*b*-P4VP it was calculated according to the following equation:

$$\left(\frac{\mathrm{d}n}{\mathrm{d}c}\right)_{\mathrm{Qx}} = \left(\frac{\mathrm{d}n}{\mathrm{d}c}\right)_{\mathrm{PEO}} \cdot w_{\mathrm{PEO}} + \left(\frac{\mathrm{d}n}{\mathrm{d}c}\right)_{\mathrm{QP4VP}} \cdot w_{\mathrm{QP4VP}} + \left(\frac{\mathrm{d}n}{\mathrm{d}c}\right)_{\mathrm{P4VP}} \cdot w_{\mathrm{P4VP}} \qquad (24)$$

where $(\mathrm{d}n/\mathrm{d}c)_i$ represents the specific refractive index increment of that particular block and w_i its respective weight fraction in the studied polymer sample.

The values for PEO (0.134 mL/g) and P4VP (0.160 mL/g) were derived from literature.[50,51,52] The specific refractive index increment of P4VP quaternized by FPBA (0.165 ml/g) was previously measured using the homopolymer by Vladimír Ďorďovič, Ph. D. Although the assumption for validity of equation (24) is fulfilled only for the Q100 that has pronounced block architecture, this model was used for estimation of d*n*/d*c* also for Q25 and Q50 samples with quaternized and non-quaternized P4VP segments arranged as a statistical copolymer. Table 7 shows both the calculation process and the final results for each of the quaternized samples.

Table 7: Estimation of dn/dc for the modified polymer samples. The degree of quaternization, DQ, the mass fraction of the respective building block i, w(i), and the resulting refractive index increment dn/dc estimation is given.

	DQ (%)	*w*(PEO)	*w*(QP4VP)	*w*(P4VP)	d*n*/d*c* (mL/g)
Q100	92	0.1206	0.8562	0.0232	0.1611
Q50	54	0.1591	0.6653	0.1756	0.1592
Q25	24	0.2147	0.3936	0.3917	0.1564

The data sets plotted in Origin are presented in Fig. 18. The data from the measurements for 30° and 40° were excluded from both graphs and calculations due to the distant values. Low angles are inherently error-prone as any impurity such as a fine dust particle can influence the measurement greatly. Table 8 contains the extracted values from both LS measurements. By dividing the obtained M_w value by the molecular weight of the polymer sample, the aggregation number N_{agg} can be determined. It shows the number of polymer chains that are assembling to create a single nanoparticle.

Table 8: Results of static and dynamic Zimm plot analysis for modified polymer samples in 0.1M HCl, with R_g being the radius of gyration, R_h the hydrodynamic radius, R_g/R_h the shape factor, M_w the weight averaged molecular weight and N_{agg} the aggregation number.

	R_g (nm)	R_h (nm)	R_g/R_h	M_w (10^5 g/mol)	N_{agg}
Q100	54 (±12%)	24	2.3	5.9 (±8.64%)	14
Q50	47 (±8.94%)	19	2.5	2.6 (±5.14%)	8
Q25*	48 (±1.38%)	19	2.5	3.4 (±0.73%)	15

*apparent values

The shape factor for all quaternized samples reached a considerably high value which is typical for elongated structures. It might suggest the presence of a flexible chain polymer coil extending into the solution (R_g/R_h = 1.505) or an ellipsoid morpohology (R_g/R_h = 0.775-4).[30]

The particles formed by Q50 and Q25 seemed to be of identical dimensions. Nevertheless, the aggregation number of Q25 is almost twice as high. This increase in density is enabled by both sterical and electrostatic factors as a smaller percentage of quaternized P4VP units allows for closer packing of polymer chains. In Q50, the repulsive interaction between the chains is rising proportionally to the number of positively charged nitrogens. These are trying to adopt a conformation with a greater distance between the adjacent charges which corresponds to the expansion of their dimensions. The particles created by the self-assembly of Q100 exhibit a similar aggregation number to those of Q25. However, the presence of quaternized pyridinium and

the hydrophobicity of FPBA above its pK_A can induce stretching of the polymer chains which results in the increase in both radii.

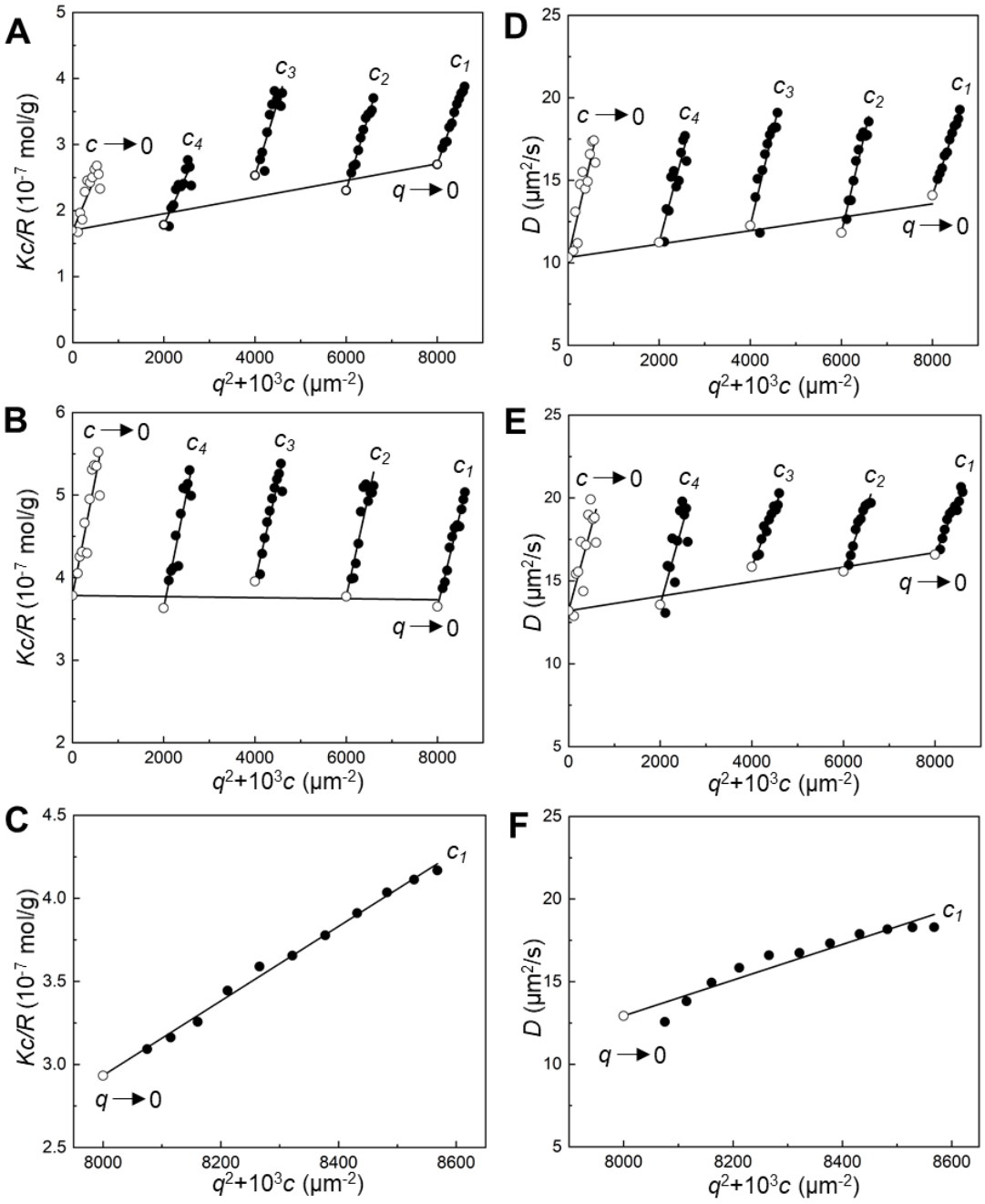

Fig. 18: The static (left) and dynamic (right) Zimm plots of (A, D) Q100 and (B, E) Q50 and a simple extrapolation for Q25 from (C) SLS and (F) DLS measurements in 0.1 M HCl for concentrations c_1, c_2, c_3 and c_4 of 0.8, 0.6, 0.4 and 0.2 mg/mL respectively

In the biological and biomedical research, phosphate-buffered saline plays an essential role as an agent that closely mimics the properties of body fluids. It is both isotonic and an effective physiological buffer since its pK_A is near the physiological pH.[53] Some of its applications are cell washing[54] or maintaining cell culture media. Its chemical

composition corresponds to the electrolytes in blood plasma and therefore it is also a suitable solvent for parenteral drug administration.[55] To enable future studies of biocompatibility of the prepared quaternized polymers such as an MTT assay, the samples dissolved in 0.1M HCl were dialysed against PBS and their self-assembly behaviour was studied via light scattering measurements.

As was partially described in section 4.2.5, during the dialysis the Q50 precipitated forming a gel-like precipitate the colour of grey tinged with green while the solutions of polymer, Q25 and Q100 in PBS were colourless and scattering. The observed radius of gyration and hydrodynamic radii for Q25 and polymer were of almost selfsame dimensions whereas the values obtained for Q100 were strikingly larger, by the factor of 6. This was in a good agreement with the notable intensity of scattering visible by the naked eye during the preparation of samples.

Table 9: Apparent size and shape parameters for Q100, Q25 and nonmodified polymer particles formed in 0.01M PBS buffer, with R_g being the radius of gyration, R_h the hydrodynamic radius, R_g/R_h the shape factor, M_w the weight averaged molecular weight and N_{agg} the aggregation number. The concentrations of Q25 and P were 0.4 mg/mL and for Q100 0.7 mg/mL.

	$R_{g,app}$ (nm)	$R_{h,app}$ (nm)	R_g/R_h	M_w (10^7 g/mol)	N_{agg}
Q100	166 (±2.54%)	95	1.75	5.1 (±4.88%)	1230
Q25	27 (±1.95%)	25	1.08	0.86 (±0.36%)	370
P	24 (±2.79%)	26	0.94	1.5 (±0.37%)	880

The Q100 and Q25 in PBS exhibited long-term stability. However, in a matter of weeks, the solution of Q25 changed colour to orange and the Q100 solution was ochre and non-transparent with a gel-like precipitate formed at the bottom of its vial. When disturbed, the precipitate was moving throughout the solution as a whole, compact unit which is demonstrated in Fig. 19.

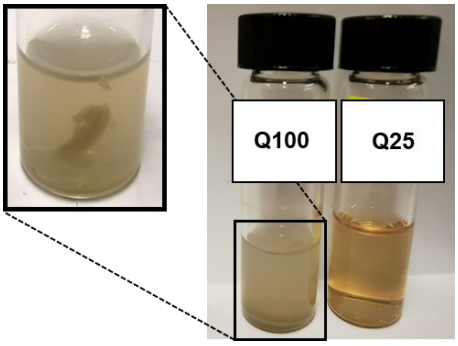

Fig. 19: Changes observed for Q100 and Q25 in 0.01M PBS buffer. Original colourless, visibly scattering solutions turned ochre in a matter of weeks and a gel-like precipitate formed in the Q100 solution.

The precipitation could be explained by crosslinking of FPBA modified polymer chains via phosphate linkage as was previously described for free phenylboronic acid[56] and quaternized P4VP homopolymer.[38] In Q25, only one quarter of P4VP units are quaternized with FPBA. Even though crosslinking causes a steep increase in the apparent molecular weight of the particles in the solution, no precipitation occurs. For Q50, the interaction between boron and phosphate is enabled by 54% of P4VP chains. Accordingly, the precipitation took place in the very course of dialysis. When Q100 is concerned, the physiological pH 7.4 of the PBS buffer might be sufficiently close to the pK_A of FPBA for a large enough fraction of FPBA to adopt the tetrahedral form which helps stabilize the solution for a certain amount of time.

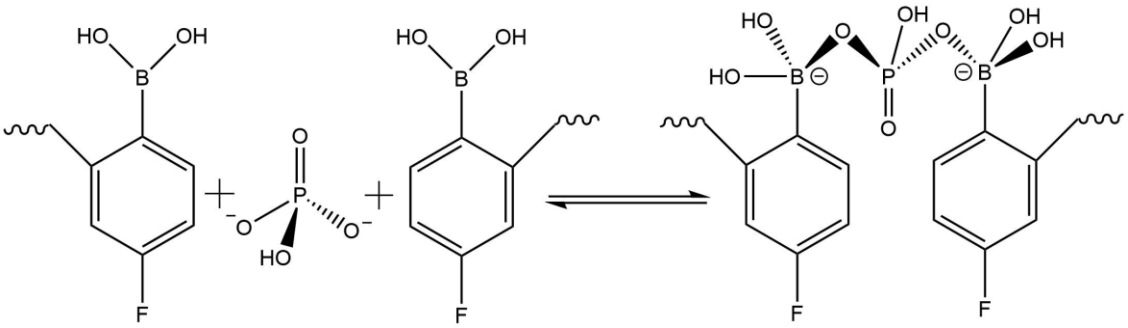

Fig. 20: Crosslinking of polymer chains via phosphate linkages

5.4 Determination of nanoparticle zeta potential

Positive zeta potential was observed for samples dissolved in 0.1M hydrochloric acid. As can be seen in Table 10, the pH of these samples was around 1 which is well above the pK_A of the pyridine group. The pyridine groups exhibit properties of a weak base and are positively charged either due to protonation from solution or quaternization by FPBA. There is an apparent decrease in zeta potential inversely proportional to the increasing degree of quaternization.

Table 10: Zeta potential of nanoparticles of the nonmodified polymer and the modified polymer samples in 0.1M HCl and water along with their standard deviations std dev. The aqueous solution was prepared by dissolving the polymer in 0.1M HCL and dialysis against water.

	ζ_{HCl} (mV)	std dev (mV)	ζ_{water} (mV)	std dev (mV)
polymer	27.1	2.69	23.3	1.73
Q25	26.1	2.44	36.3	1.46
Q50	20.7	0.893	41.0	1.48
Q100	13.2	1.74	49.1	2.15

As was previously seen, the presence of modified P4VP containing hydrophobic fluorine greatly affects the solubility of these samples. In the ^{1}H NMR spectra, the P4VP

hydrogens are clearly visible only for Q25, their intensity is significantly reduced in Q50 spectra and for Q100 they disappeared completely. This suggests the presence of core-shell micelles with P4VP core stabilized by a PEO shell. It also corresponds to the decreasing zeta potential since the positively charged pyridine groups might be shielded by the surrounding PEO chains. The effect is the most striking for Q100.

In a neutral solution, a zero zeta potential would be expected for the nonmodified polymer sample. Yet due to dialysis from HCl, the pH of the aqueous solutions (Table 3) was around 5, close to the pK_A of P4VP. Unlike a low-molecular weak acid, a macromolecular polyelectrolyte exhibits a more complex ionization behaviour. Therefore it cannot be simply stated that at the pH equal to pK_A of P4VP, 50% of P4VP chains are ionized. Nevertheless, the positive zeta potential is probably caused either due to protonation of P4VP nitrogen in the still acidic solution or retention of a positive charge on some of the PEO oxygens throughout the dialysis process. For quaternized samples, the zeta potential is increasing proportionally to the degree of quaternization placing a permanent positive charge on a rising percentage of P4VP nitrogens. The zeta potential is also affected by the decreased ionic strength of the aqueous solution in comparison to the 0.1M HCl.[57,58]

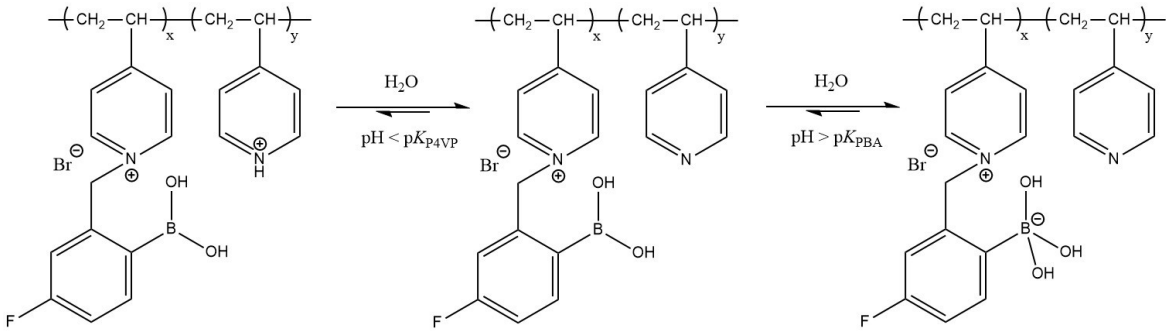

Fig. 21: The effect of pH on the ionization equilibria of polymer polyelectrolytes

A more in-depth investigation into the zeta potential of Q25 as a function of pH was carried out. The experimental data were fitted with a sigmoidal function using Origin software. The initial high positive zeta potential decreases by half when the pH reaches 4.27. This is caused by multiple factors. Firstly, the pH is getting closer to the pK_A of pyridine which is being deprotonated. Secondly, during titration with a strong base, the ionic strength of the studied solution is increasing and the zeta potential is lowered. Below the pH 7.73, Q25 exhibits a negative zeta potential that slightly lowers once the pK_A of PBA is crossed. At the pH 9.35, most PBA groups adopt the anionic form and the zeta potential remains constant despite further changes in pH indicating the growing negative charge in the proximity of the remaining trigonal PBAs effectively repels hydroxide ions before they could participate in the equilibrium reaction.

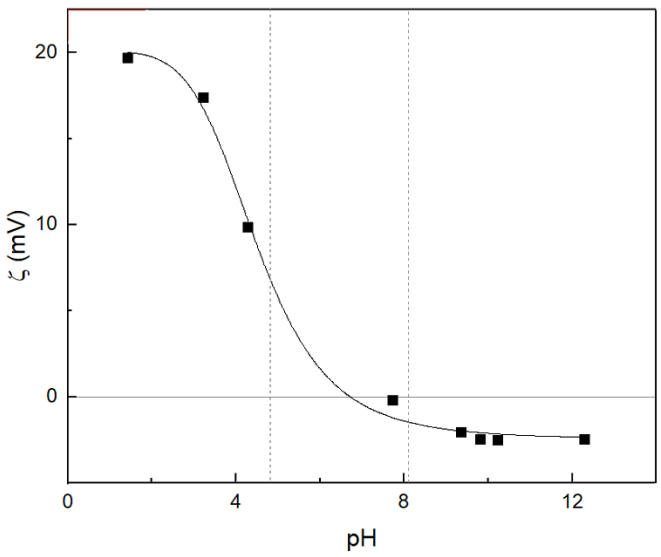

Fig. 22: The pH dependance of zeta potential of Q25. 2 mL of solution (1 g/L) in 0,1M HCl titrated by 1M NaOH, the pK_A of P4VP and 4-fluorophenylboronic acid have been marked.

5.5 Nanoparticle size and shape determination by AFM

The cleavage plane of the freshly peeled mica is hydrophilic and negatively charged. The surface was dip coated in a relatively concentrated (approximately 0.5 g/L) micellar solution which resulted in a rather dense deposition of particles. These were positively charged due to quaternization placing a permanent positive charge on nitrogen and the protonated P4VP chains. Immobilization on the surface of mica leads to deformation of particles, sometimes colloquially termed as pancake deformation. The core is affected by electrostatic interaction, while the soluble shell-forming blocks spread on the hydrophilic mica surface and the favourable interactions with mica along with the entropy effect cause them to stretch.[59] Even in tapping mode, the interaction between the slightly negatively charged silicon nitride probing tip and polycation of P4VP also elongates the dimension in the direction of the scan creating an impression of ellipsoidal shape. In conlusion, the size and shape of particles in solution and adsorbed on a surface differ substantially and a comparison must be drawn carefully.

A presence of a fraction of large micellar aggregates above 80 nm in height is evident on all of the AFM scans. Seeing that these were not observed during the light scattering experiment, it is suspected that their formation occurs during drying after the sample is deposited on the surface. Undoubtedly, overwhelming majority of particles exhibit significantly smaller dimensions. Coincidentally with LS, there was no striking difference in the values observed for the statistically predominant particles. The average height was 30-40 nm for Q100, 20-30 nm for Q50 and 30-40 nm for Q25. Nonetheless, the cross sections have been chosen in a way to present both the majority and the micellar clusters (Fig. 24). Possibly, the cluster formation could be avoided by sufficient diluting of the deposited sample.[60]

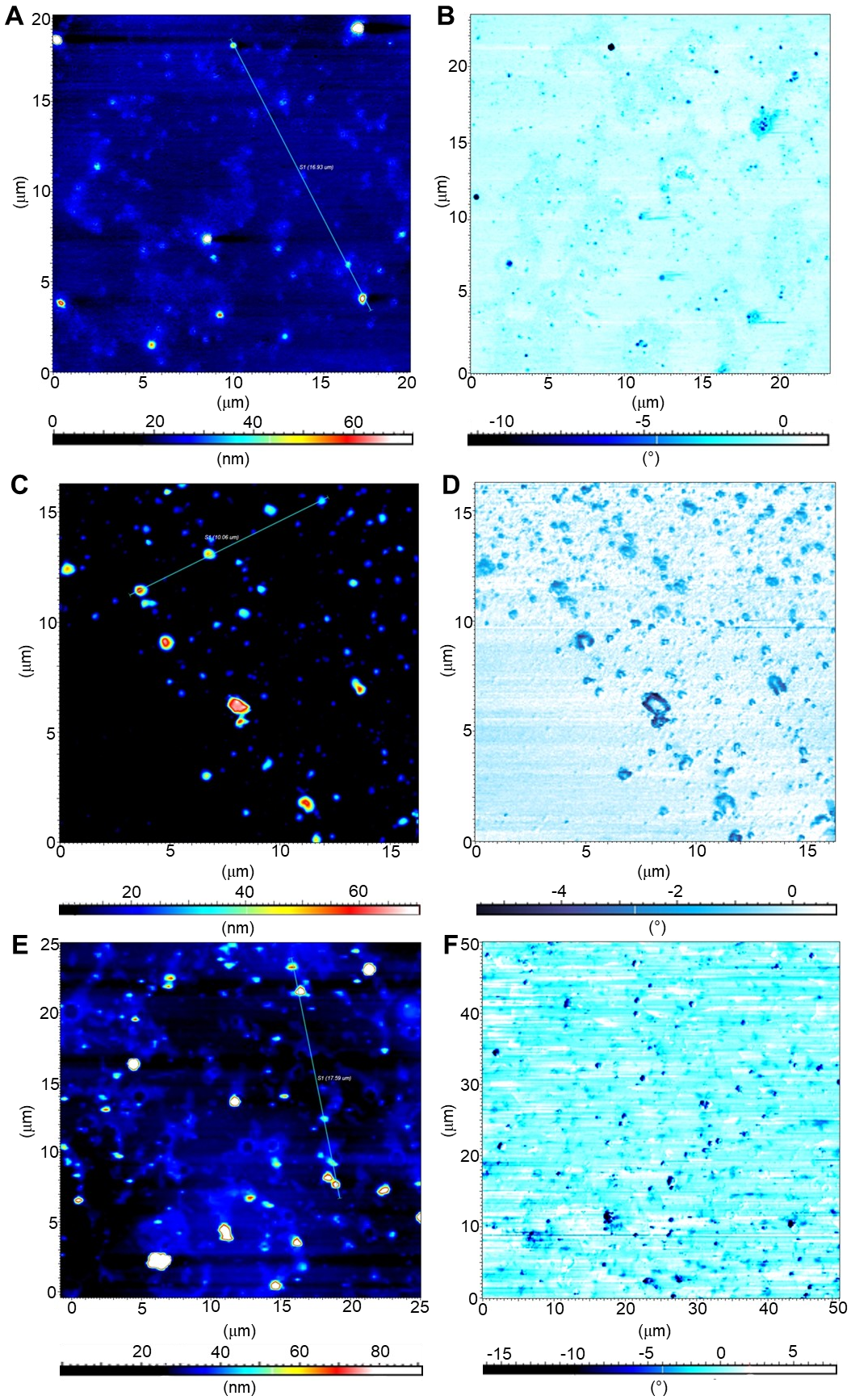

Fig. 23: AFM images of height scans (left) and phase scans (right) of (A, B) Q100, (C,D) Q50 and (E, F) Q25 in 0.1M HCl (0.5 g/L). The cross sections along the white lines are shown in Fig. 24

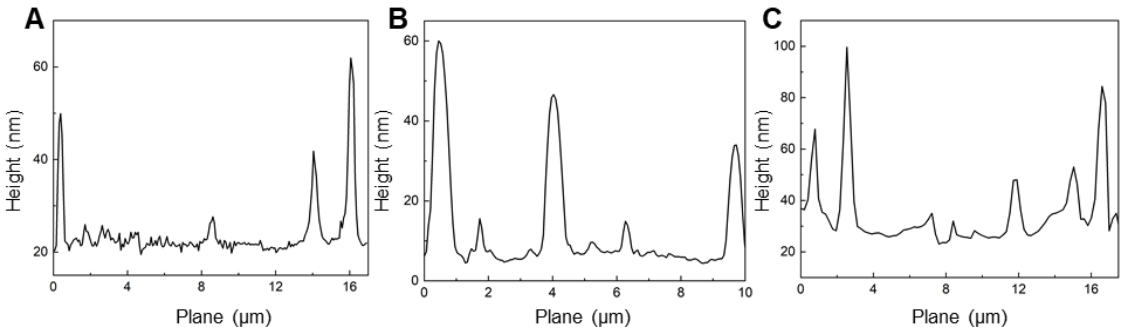

Fig. 24: The cross sections of height scans for (A) Q100, (B) Q50 and (C) Q25 along the white lines

To visualize a true representation of particles in solution for a direct comparison with LS data, in situ cryogenic transmission electron microscopy could be utilized. However, the kinetics seem to play an important role in the behaviour of the studied polymer. Therefore, the compared samples should be ideally prepared and measured at the same time.

5.6 UV-Vis absorbance and steady-state fluorescence experiments

UV-Vis absorbance and steady-state fluorescence experiments were performed to probe the photophysical changes in the polymeric micelles upon crosslinking with one of the two model compounds, crocin and gossypol-acetic acid. Their structures are shown in Fig. 25. The aim was to study the influence of length and structure of these functional diols on the formed ester bonds. In theory, the crosslinks produced by crocin should be both longer and more flexible since its structure provides more opportunities for torsional motion.

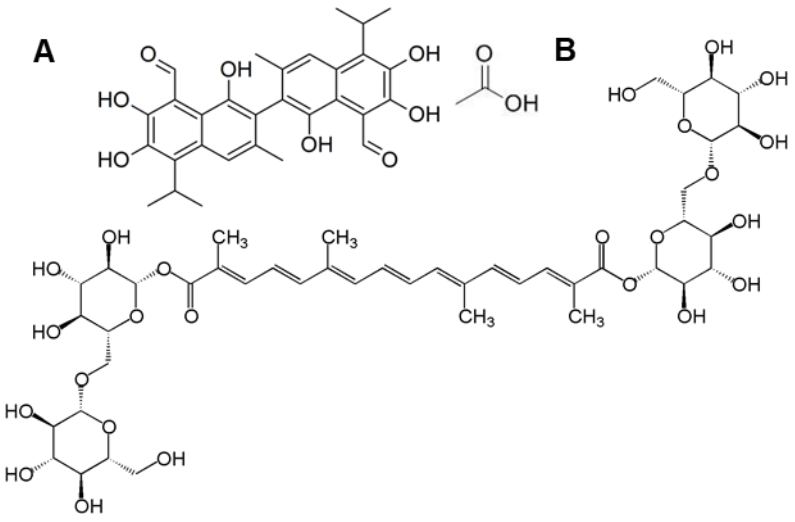

Fig. 25: Structures of crosslinking agents (A) gossypol-acetic acid and (B) crocin

The absorption spectra of the stock solutions of crocin and gossypol-acetic acid (further denoted as gossypol) were consistent with those reported in literature.[24,61] The modified polymer itself exhibited strong absorption bands that were attributed to the phenylic groups and their π to π* transitions. The first in the near UV region at 306 nm with a broad shoulder suggesting an existence of a non-separated second peak centered at 385 nm. A weak absorption peak was also observed at 620 nm. (Fig. 27)

To three separate samples of Q100 in 0.1M NaOH, 0.5, 1 and 2 molar equivalents of the respective natural molecule were added to examine and compare the effect of increasing concentration of crosslinking agents on the formation of ester bonds. Despite the anticipated results, only a small increase in the overall absorption was detected with no common trend related to the increasing concentration of therapeutic agent. A solution of Q100 with 20 molar equivalents of crocin showed a more pronounced increase in the absorption in the areas of previously determined absorption maxima of crocin. It was disputable whether this change originated from the increasing concentration of crocin itself or its interaction with PBA. Considering the equilibrium constant of the dynamic formation of esterified boronate ester species remains unknown, a more pronounced molar excess might be needed to increase efficiency of binding.

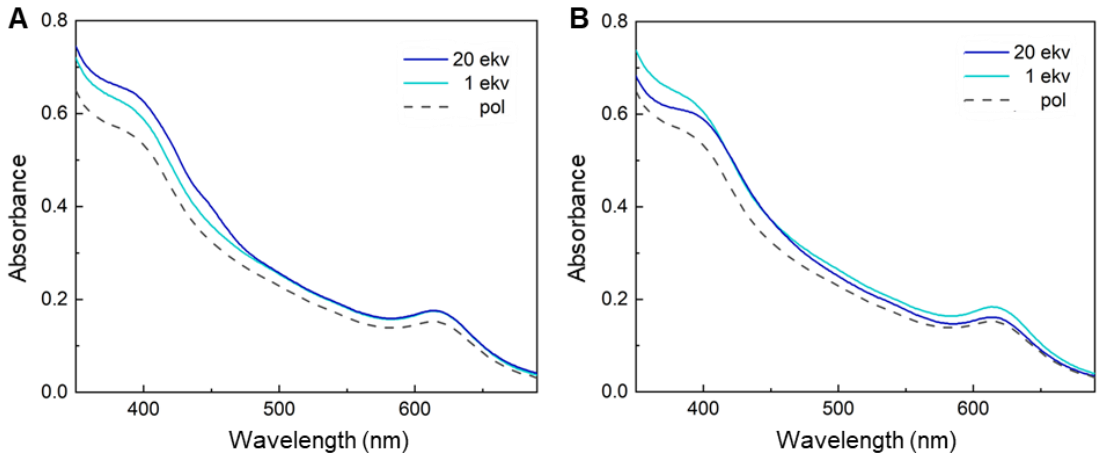

Fig. 26: The absorbance of micellar solution with the addition of (A) crocin and (B) gossypol. The dashed line represents the absorbance of a pure polymer sample.

In conclusion, the unpredicted strong absorption of the studied polymer sample controlled the appearance of the absorbance spectra. Even though phenomenon hindered the intended study of interaction between the selected funcional diols and modified polymer sample, it revealed an interesting property of the modified polymer. To gain in-depth insight into this matter, the absorption of the polymer sample and more importantly its development in time was investigated. The weak absorption band located at 620 nm was gradually moving towards lower wavelengths (612 nm) and its intensity was decreasing, it disappeared completely in 8 days. The peak located in the near UV region and its broad shoulder demonstrated opposite behaviour with continuous increase in their intensity.

The solution of Q100 in 0.05M NaOH appeared to be coloured in a dark shade of yellow. That can be related to the broad absorption band centered at 385 nm.

Due to the broadness, the absorbed wavelengths reach the value 430 nm which is well in the region of visible violet light.[62] Thus, the perceived colour of the solution is the complimentary yellow.

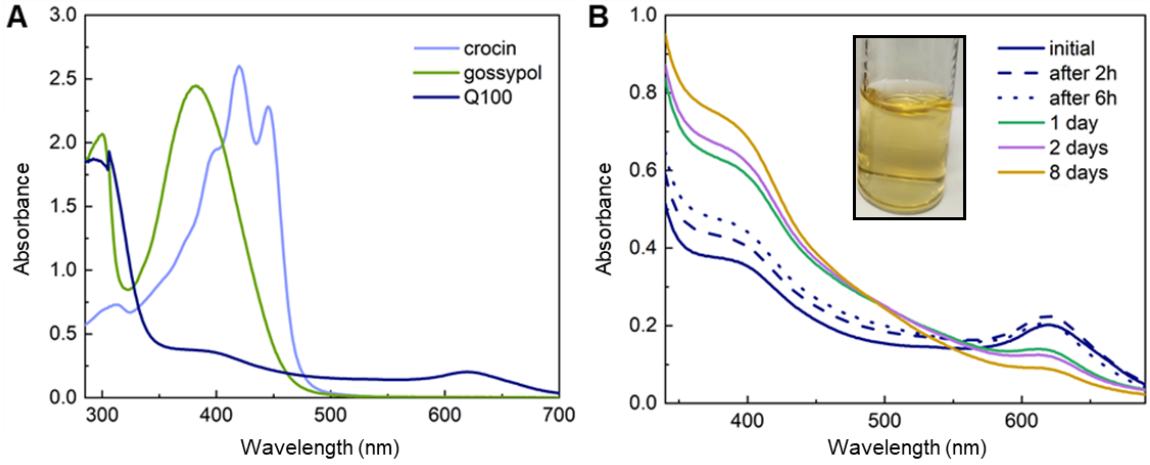

Fig 27: The (A) absorbance spectra of crocin, gossypol and Q100 and (B) time development of the absorbance of Q100.

Similar observations were made using the complementary method of fluorescence spectroscopy. The emission and excitation spectral profiles of crocin, gossypol and Q100 (Fig. 28) were measured in the region of interest. Upon the addition of 0.5, 1 and 2 molar equivalence of gossypol or crocin to the studied solution of Q100, the measured intensity barely changed with no apparent trend relating to the concentration of the respective functional diol. Nonetheless, for Q100 the dependance of intensity on time was again investigated and the measurements were repeated the next day and in a week. Following the same pattern as with the UV-Vis measurements, the intensity was gradually increasing.

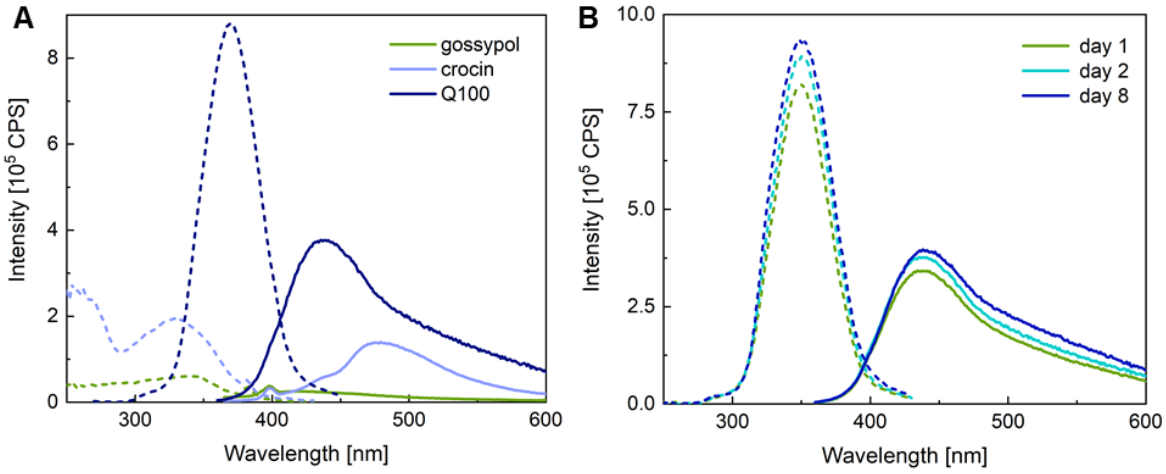

Fig. 28: The excitation (dashed line) and emission (solid line) fluorescence spectra of (A) gossypol, crocin and Q100 and (B) the time development of the Q100 fluorescence spectra. The concentration of Q100 was 1 mg/mL in 0.05M NaOH.

It has been shown that a poly(4-vinyl-N-n-butyl-pyridinium bromide) is a charge-transfer complex with a relatively low transition energy resulting in green solution upon dissolution in ethanol and that the colour is not very sensitive to change of the N-substitient.[63] This corresponds to the observations made for quaternized polymer samples in a more concentrated 0.1M NaOH. However, the the solution in 0.05M NaOH has shown a rather yellowish colour. A coordination between the boron in the PBA moiety and the nitrogen originating from the P4VP building block can affect the photophysical properties of polymeric micelles. Nitrogen acts as a Lewis base and can donate electron density to the electron-defficient boron forming a B-N Lewis pair. Such behaviour has been reported for a large number of low-molecular organoboron compounds[64] and also copolymers.[65,66] The association and possible photodissociation of such B-N interactions modulates the electron density distribution and slightly alters orbital energies.[67] The higher concentration of hydroxide anions shifts the equilibrium reaction more towards the tetrahedral and no longer electron-deficient hydroxyboronate species, reducing opportunities for B-N pair formation in comparison to a more dilute basic solution.

6. Conclusion

1. A stimuli-responsive diblock hydrophilic copolymer PEO-*b*-P4VP was functionalized via post-polymerization quaternization reaction with 2-bromomethyl-4-fluorophenylboronic acid in tetrahydrofurane. Three different degrees of quaternization were attempted, 25, 50 and 100%. Products were isolated by precipitation and filtration in the form of light brown (Q100), brown (Q50) and light yellow (Q25) solid. The newly introduced functional group gave rise to a change in solubility. While the nonmodified polymer was not soluble in the solution of sodium hydroxide even when heated to 60 °C, the Q100 dissolved the fastest in basic conditions and was the most stable. This is attributed to the hydrophilicity of the hydroxyboronate species formed above the pK_A of FPBA which helps solubilize the polymer and stabilizes it in solution.
2. ^{1}H NMR in MeOD/D_2O was used to determine the degree of quaternization. The value of one was assigned to the integral of PEO. Due to the hydrophobicity of fluorine-modified PBA, it was compared to the integrated signal of methylene linker to quantify the number of functionalized P4VP units. A 24, 54 and 92% quaternization was confirmed for Q25, Q50 and Q100 respectively. Peaks associated with P4VP were attenuated in the acidic environment proportionally to the degree of quaternization and dissapeared completely for Q100, suggesting the formation of kinetically frozen nanoparticles with PEO shell stabilized P4VP core. The FTIR spectra displayed vibrational bands characteristic for the incorporation of boronic acid such as the O-H and B-O stretching motions. The ratio between the intensities of peak for quaternized and nonmodified pyridine indicated the rising degree of quaternization in agreement with the results from ^{1}H NMR spectra.
3. An estimation of specific refractive index increment was calculated for each sample. Data from SLS and DLS were treated with static and dynamic Zimm plot analysis. The radius of gyration was approximately 50 nm, twice the hydrodynamic radius, and slightly increasing with the degree of quaternization due to electrostatic repulsion between the modified chains. The samples were dialysed against PBS. Q50 precipitated in the course of dialysis and the substantial 3-fold increase in Q100 micelle radii indicated chain crosslinking via phosphate linkages. In HCl, Q25 exhibited the largest zeta potential +26 mV. The decrease towards higher degrees of quaternization was linked to insufficient solubility of quaternized P4VP as was also observed via ^{1}H NMR spectroscopy and high ionic strength of the solution. In water, the zeta potential of Q100 was +49 mV and the value gradually decreased with the decreasing quaternization. The average height acquired by AFM was 30 nm for all the samples, however, a fraction of larger aggregates formed on the surface, probably during sample preparation.
4. UV-Vis absorbance and steady-state fluorescence experiments were performed to probe the photophysical changes in the polymeric micelles upon crosslinking with one of the two model compounds, crocin and gossypol-acetic acid. Only a large excess of the drug resulted in a significant altering of the spectra which was overall dominated by strong absorption and fluorescence of the prepared polymeric micelles. These were investigated repeatedly and a gradual increase in the intensity was observed.

References

1. Grumezescu, A. M., & Varga, M. (2016). Self-assembly of nanobiomaterials. In *Fabrication and self-assembly of nanobiomaterials: applications of nanobiomaterials*. Amsterdam: Elsevier/William Andrew.
2. Bhushan, B., & Lu, W. (2012). Self-assembly of Nanostructures. In *Encyclopedia of Nanotechnology*. New York: Springer.
3. Jana, S., & Uchman, M. (2020). Poly(2-oxazoline)-based stimulus-responsive (Co)polymers: An overview of their design, solution properties, surface-chemistries and applications. *Progress in Polymer Science*, *106*, 101252.
4. Laschewsky, A. (2014). Structures and Synthesis of Zwitterionic Polymers. *Polymers*, *6*(5), 1544–1601.
5. Kennemur, J. G. (2019). Poly(vinylpyridine) Segments in Block Copolymers: Synthesis, Self-Assembly, and Versatility. *Macromolecules*, *52*(4), 1354–1370.
6. Wu, Y., Wang, K., Tan, H., Xu, J., & Zhu, J. (2017). Emulsion Solvent Evaporation-Induced Self-Assembly of Block Copolymers Containing pH-Sensitive Block. *Langmuir*, *33*(38), 9889–9896.
7. Alconcel, S. N. S., Baas, A. S., & Maynard, H. D. (2011). FDA-approved poly(ethylene glycol)–protein conjugate drugs. *Polymer Chemistry*, *2*(7), 1442.
8. Younes, M., et al. (2018). Refined exposure assessment of polyethylene glycol (E 1521) from its use as a food additive. *EFSA Journal*, *16*(6).
9. Fruijtier-Pölloth, C. (2005). Safety assessment on polyethylene glycols (PEGs) and their derivatives as used in cosmetic products. *Toxicology*, *214*(1-2), 1–38.
10. Alconcel, S. N. S., Baas, A. S., & Maynard, H. D. (2011). FDA-approved poly(ethylene glycol)–protein conjugate drugs. *Polymer Chemistry*, *2*(7), 1442.
11. Savjani, K. T., Gajjar, A. K., & Savjani, J. K. (2012). Drug Solubility: Importance and Enhancement Techniques. *ISRN Pharmaceutics*, *2012*, 1–10.
12. Schmidt, B. V. K. J. (2018). Double Hydrophilic Block Copolymer Self-Assembly in Aqueous Solution. *Macromolecular Chemistry and Physics*, *219*(7), 1700494.
13. Lu, Y., Zhang, E., Yang, J., & Cao, Z. (2018). Strategies to improve micelle stability for drug delivery. *Nano Research*, *11*(10), 4985–4998.
14. Xie, C., et al. (2015). Synthesis of drug-crosslinked polymer nanoparticles. *Polymer Chemistry*, *6*(10), 1703–1713.
15. Li, Y., et al. (2019). Dual Stable Nanomedicines Prepared by Cisplatin-Crosslinked Camptothecin Prodrug Micelles for Effective Drug Delivery. *ACS Applied Materials & Interfaces*, *11*(23), 20649–20659.
16. Greish, K. (2007). Enhanced permeability and retention of macromolecular drugs in solid tumors: A royal gate for targeted anticancer nanomedicines. *Journal of Drug Targeting*, *15*(7-8), 457–464.
17. Maeda, H. (2015). Toward a full understanding of the EPR effect in primary and metastatic tumors as well as issues related to its heterogeneity. *Advanced Drug Delivery Reviews*, *91*, 3–6.
18. Hall, D. G. (2012). Structure, Properties, and Preparation of Boronic Acid Derivatives. Overview of Their Reactions and Applications. In *Boronic Acids: Preparation and Applications in Organic Synthesis, Medicine and Materials*. Somerset: Wiley.
19. Zarzeczańska, D., et al. (2017). Fluorinated Boronic Acids: Acidity and Hydrolytic Stability of Fluorinated Phenylboronic Acids. *European Journal of Inorganic Chemistry*, *2017*(38-39), 4493–4498.

20. Marinaro, W. A., et al. (2015). Interaction of Model Aryl- and Alkyl-Boronic Acids and 1,2-Diols in Aqueous Solution. *Journal of Pharmaceutical Sciences*, *104*(4), 1399–1408.
21. Hebel, M., et al. (2019). Sequence Programming with Dynamic Boronic Acid/Catechol Binary Codes. *Journal of the American Chemical Society*, *141*(36), 14026–14031.
22. Stubelius, A., Lee, S., & Almutairi, A. (2019). The Chemistry of Boronic Acids in Nanomaterials for Drug Delivery. *Accounts of Chemical Research*, *52*(11), 3108–3119.
23. Escribano, J., et al. (1996). Crocin, safranal and picrocrocin from saffron (Crocus sativus L.) inhibit the growth of human cancer cells in vitro. *Cancer Letters*, *100*(1-2), 23–30.
24. Foss, B. J., et al. (2005). Hydrophilic carotenoids: surface properties and aggregation behavior of a highly unsaturated carotenoid lysophospholipid. *Chemistry and Physics of Lipids*, *134*(2), 85–96.
25. Colapietro, A., et al. (2019). Crocetin and Crocin from Saffron in Cancer Chemotherapy and Chemoprevention. *Anti-Cancer Agents in Medicinal Chemistry*, *19*(1), 38–47.
26. Jagt, D. V., Deck, L., & Royer, R. (2000). Gossypol Prototype of Inhibitors Targeted to Dinucleotide Folds. *Current Medicinal Chemistry*, *7*(4), 479–498.
27. Xiong, J., et al. (2017). Gossypol has anti-cancer effects by dual-targeting MDM2 and VEGF in human breast cancer. *Breast Cancer Research*, *19*(1).
28. Heleg-Shabtai, V., et al. (2015). Gossypol-Cross-Linked Boronic Acid-Modified Hydrogels: A Functional Matrix for the Controlled Release of an Anticancer Drug. *Langmuir*, *31*(7), 2237–2242.
29. Øgendal, L. H. (2017). *Light Scattering Demystified: Theory and Practice.* University of Copenhagen.
30. Schärtl, W. (2007). Fundamental Concepts. In *Light Scattering from Polymer Solutions and Nanoparticle: Dispersions*. Berlin: Springer.
31. Atkins, P. W., Trapp, C. A., & Paula, J. D. (2010). *Physical chemistry*. Oxford: Oxford Univ. Press.
32. Schröder, E., Müller, G., & Arndt, K.-F. (1989). *Polymer characterization*. Berlin: Akademie-Verlag Berlin.
33. Severn, G. D. (2018). Molecular Spectroscopy of N2 version 2.0. *Physics 272 Laboratory Experiments*. Retrieved August 11, 2020, from http://home.sandiego.edu/~severn/p272/molecular_spectroscopy.html
34. Němec, I., Štícha M., Tošner, Z. (2020). Fundamantals of molecular spectroscopy, [lecture], Prague, Charles Univerity, Faculty of Science.
35. Facey, G. (2008). ^{1}H NMR with ^{11}B Decoupling. *University of Ottawa NMR Facility Blog*. Retrieved August 11, 2020, from http://u-of-o-nmr-facility.blogspot.com/2008/04/1-h-nmr-with-11-b-decoupling.html
36. Koltzenburg, S., Maskos, M., & Nuyken, O. (2017). *Polymer Chemistry*. Heidelberg: Springer-Verlag Berlin.
37. Kawaguchi, S., Winnik, M. A., & Ito, K. (1996). ^{1}H NMR Study of Dispersion Copolymerization of n-Butyl Methacrylate with Poly(ethylene oxide) Macromonomer in Deuterated Methanol−Water. *Macromolecules*, *29*(13), 4465–4472.
38. Ďorďovič, V., Vojtová, J., Jana, S., & Uchman, M. (2019). Charge reversal and swelling in saccharide binding polyzwitterionic phenylboronic acid-modified poly(4-vinylpyridine) nanoparticles. *Polymer Chemistry*, *10*(40), 5522–5533.

39. Sasaki, K., et al. (2013). Characteristic Sorption of $H_3BO_3/B(OH)_4^-$ on Magnesium Oxide. *Materials Transactions*, *54*(9), 1809–1817.
40. Pal, S. (2018). Pyridine: A Useful Ligand in Transition Metal Complexes. In *Pyridine*. IntechOpen. Available from: https://www.intechopen.com/books/pyridine/pyridine-a-useful-ligand-in-transition-metal-complexes
41. Stanković, D., et al. (2011). Determination of Copper in Water by Anodic Stripping Voltammetry Using Cu-DPABA–NA/GCE Modified Electrode. *International Journal of Electrochemical Science.* 6. 5617-5625.
42. Kawaguchi, S., Winnik, M. A., & Ito, K. (1996). ^{1}H NMR Study of Dispersion Copolymerization ofn-Butyl Methacrylate with Poly(ethylene oxide) Macromonomer in Deuterated Methanol−Water. *Macromolecules*, *29*(13), 4465–4472.
43. Chowdhury, P., Saha, S. K., & Bayen, S. P. (2013). Synthesis of Quaternized poly(4-Vinyl Pyridine) and the Study of its Ion Exchange Property. *Journal of Macromolecular Science, Part A*, *50*(9), 976–982.
44. Vengatesan, S., et al. (2015). Novel cross-linked anion exchange membrane based on hexaminium functionalized poly(vinylbenzyl chloride). *RSC Advances*, *5*(35), 27365–27371.
45. Wang, Y., et al. (2013). Highly swellable ultrathin poly(4-vinylpyridine) multilayer hydrogels with pH-triggered surface wettability. *Soft Matter*, *9*(39), 9420.
46. Katcka, M., & Urbanski, T. (1964). Infrared Absorption Spectra of Quaternary Salts of Pyridine. *Bulletin De L'Académie Polonaise Des Sciences, 12*(9), des sciences chimiques, 615-621.
47. Brewer, S. H., et al. (2004). Infrared Detection of a Phenylboronic Acid Terminated Alkane Thiol Monolayer on Gold Surfaces. *Langmuir, 20*(13), 5512-5520.
48. Faniran, J. A., & Shurvell, H. F. (1968). Infrared spectra of phenylboronic acid (normal and deuterated) and diphenyl phenylboronate. *Canadian Journal of Chemistry, 46*(12), 2089-2095. doi:10.1139/v68-341
49. Is it alright to estimate d*n*/d*c* in SLS measurements? *Materials Talks*, Malvern Instruments. Retrieved August 12, 2020, from https://www.materials-talks.com/
50. Huglin, M. B. (1991). Specific refractive index increments of polymers in dilute solution, in: Brandrup, J., Immergut, E.H. (Eds.), *Polymer Handbook*, John Wiley, New York, pp. VII/409–VII/471
51. Bello, A., & Guzman, G. (1966). Specific refractive index increments of polymers and copolymers in several solvents. *European Polymer Journal*, *2*(1), 85–91.
52. Tumolo, T., Angnes, L., & Baptista, M. S. (2004). Determination of the refractive index increment (dn/dc) of molecule and macromolecule solutions by surface plasmon resonance. *Analytical Biochemistry, 333*(2), 273-279.
53. Mackintosh, S. (2012). Buffers and Their Physiological Importance. Retrieved August 11, 2020, from https://library.uams.edu/assets/COM/BioChem/AminoAcidsPeptides/Amino_Acids_and_Peptides3.html
54. Yoon, S., Kim, Y. K., & Mofrad, M. R. (2013). Mechanobiological Approaches for the Control of Cell Motility. *Microfluidic Cell Culture Systems,* 105-136.
55. Zunino, S. J., et al. (2012). Oral or parenteral administration of curcumin does not prevent the growth of high-risk t(4;11) acute lymphoblastic leukemia cells

engrafted into a NOD/SCID mouse model. *International Journal of Oncology, 42*(2), 741-748.
56. Bosch, L., Fyles, T., & James, T. (2004). Binary and ternary phenylboronic acid complexes with saccharides and Lewis bases. *Tetrahedron, 60*(49), 11175-11190.
57. Mcconaughy, S. D., et al. (2008). Structural Characterization and Solution Properties of a Galacturonate Polysaccharide Derived fromAloe veraCapable of in Situ Gelation. *Biomacromolecules, 9*(2), 472-480.
58. Carneiro-Da-Cunha, et al. (2011). Influence of concentration, ionic strength and pH on zeta potential and mean hydrodynamic diameter of edible polysaccharide solutions envisaged for multinanolayered films production. *Carbohydrate Polymers, 85*(3), 522.
59. Štěpánek, M., et al. (2003). Light Scattering, Atomic Force Microscopy and Fluorescence Correlation Spectroscopy Studies of Polystyrene-block-poly(2-vinylpyridine)-block-poly(ethylene oxide) Micelles. *Collection of Czechoslovak Chemical Communications, 68*(11), 2120-2138.
60. Humpolíčková, J., et al. (2003). Fluorescence Correlation Spectroscopy Using Octadecylrhodamine B as a Specific Micelle-Binding Fluorescent Tag; Light Scattering and Tapping Mode Atomic Force Microscopy Studies of Amphiphilic Water-Soluble Block Copolymer Micelles†,‡. *Langmuir, 19*(10), 4111-4119.
61. Jia, G., et al. (2009). An improved ultrasound-assisted extraction process of gossypol acetic acid from cottonseed soapstock. *AIChE Journal*, *55*(3), 797–806.
62. Visible Spectroscopy, [online lecture], University of California, Irvine Retrieved August 11, 2020, from http://faculty.sites.uci.edu/chem2l/files/2011/04/RDGVISSpec.pdf
63. Boucher, E. A., & Mollett, C. C. (1982). Coloured and colourless charge-transfer complexes of small and polymeric quaternary pyridinium bromides. *Journal of the Chemical Society, Faraday Transactions 1: Physical Chemistry in Condensed Phases*, *78*(5), 1401.
64. Mellerup, S. K., & Wang, S. (2019). Boron-based stimuli responsive materials. *Chemical Society Reviews*. The Royal Society of Chemistry. *48*, 3537-3549.
65. Iovine, P. M., Fletcher, M. N., & Lin, S. (2006). Condensation of Arylboroxine Structures on Lewis Basic Copolymers as a Noncovalent Strategy toward Polymer Functionalization. *Macromolecules*, *39*(19), 6324–6326.
66. Gaballa, H., Shang, J., Meier, S., & Theato, P. (2018). The glucose-responsive behavior of a block copolymer featuring boronic acid and glycine. *Journal of Polymer Science Part A: Polymer Chemistry*, *57*(3), 422–431.
67. Matsuo, K., Saito, S., & Yamaguchi, S. (2014). Photodissociation of B–N Lewis Adducts: A Partially Fused Trinaphthylborane with Dual Fluorescence. *Journal of the American Chemical Society*, *136*(36), 12580–12583.